Study on Endothelial Network Formation in Fluidic Multilayered Myoblast Sheet

Ngo Xuan Trung

September 2013

Study on Endothelial Network Formation in Fluidic Multilayered Myoblast Sheet

A dissertation submitted to

THE GRADUATE SCHOOL OF ENGINEERING SCIENCE

OSAKA UNIVERSITY

In fulfillment of the requirements for the degree of

DOCTOR OF PHILOSOPHY IN ENGINEERING

By

Ngo Xuan Trung

September 2013

Preface

This study was conducted under the co-supervision of Professors Masahito Taya and Masahiro Kino-oka at the Division of Chemical Engineering, Graduate School of Engineering Science, Osaka University, from 2008 to 2013.

The main objective of this thesis is to understand the mechanism of endothelial behaviors during network formation process, the initial step of angiogenesis, in a fluidic multilayered myoblast sheet, through the construction of a novel 3D *in vitro* culture system which imitates the *in vivo* angiogenesis using cell sheet engineering. The effects of various factors, such as the thickness of the cell sheet, the culture time, and the density of endothelial cells on network formation process are discussed. The author hopes that the findings in this work will offer a deeper understanding of cell behaviors in 3D structures and open the way to future application in regenerative medicine.

Ngo Xuan Trung

Division of Chemical Engineering

Graduate School of Engineering Science

Osaka University

Toyonaka, Osaka 560-8531, JAPAN

Contents

Abstract

The autologous transplantation of a myoblast cell sheet is emerging as a promising technique for treating myocardial infarction due to the cells' ability to secrete some important cytokines, which improve heart function via the facilitation of angiogenesis and the attraction of progenitors to the infarcted area. The process- and quality- controls are critical steps for realizing in practice a broad cure using myoblast sheet. The clarification of the mechanism by which the endothelial cells of the host migrate into the transplanted myoblast sheets leads to the enhancement of transplant quality. Therefore, in this study, the author aimed to construct a novel 3D *in vitro* culture system imitating the *in vivo* angiogenesis, to understand the mechanism of the network formation of endothelial cells (target cells) in a fluidic multilayered myoblast sheet (packed cells), and to develop observation and image processing methods to analyze cell behaviors toward application of these methods in quality control.

In chapter 1, a procedure for fabricating a multilayered cell sheet was developed using a temperature-responsive surface and a stamp system. Confocal laser scanning microscopy and image processing revealed that the fluidity of a multilayered sheet of human skeletal muscle myoblasts (HSMMs) can be estimated analogy to molecular diffusivity, and the sheet fluidity was changed upon addition of dermal fibroblasts.

In chapter 2, a novel 3D *in vitro* culture system was developed, in which green fluorescent protein expressing human umbilical vein endothelial cells (GFP-HUVECs) were cultured under HSMM sheets with different layer numbers to vary the thickness of the cell sheet. The difference in the thickness of the cell sheet caused different endothelial behaviors, such as cell detachment on the top of the monolayer sheet, island-shape aggregate on the top of the three-layered sheet, and network formation in the middle and basal layer of the five-layered and seven-layered sheet,

respectively, during 96 h of incubation. The thickness of the HSMM sheet, which can be controlled by the number of layers in the cell sheet, is therefore an important factor that affects endothelial behavior in the cell sheet.

In chapter 3, an image processing method was developed to quantitatively analyze the dynamic behaviors of endothelial cells during the network formation process. The HUVECs at the bottom of the HSMM sheet elongated, actively migrated upward, encountered and connected to form network in the middle of the HSMM sheet from 0 to 96 h of incubation, and finally degraded at 120 h. Non-networked HUVECs continued to migrate to the top of the sheet, indicating the spatial habitation of HUVECs in the cell sheet. An evaluation of the network extension using image processing showed that initial density of HUVECs strongly affected the extent of endothelial network formation.

Overall, this study successfully established a novel 3D *in vitro* culture system imitating *in vivo* angiogenesis with different observation and quantitative analysis methods applicable in quality control. The mechanism of endothelial behaviors during network formation, the initial step of angiogenesis, was clarified by taking into consideration various factors, such as the thickness of the cell sheet, the culture time, and the density of the endothelial cells. The broad, well-connected endothelial network obtained in multilayered myoblast sheet as prevascularization is likely to be successfully applied in regenerative medicine in the future.

General Introduction

Cell sheet technology

Cell sheet technology is an advanced scaffold-free tissue engineering methodology using temperature-responsive culture surface (**Fig. 1**). A layer of *N*-isopropylacrylamide (IPAAm) monomer is applied on a normal culture surface and then subjected to electron beam irradiation, leading to the covalent immobilization of the polymer (PIPAAm) onto the surface (Okano *et al*., 1993). An interesting characteristic of the PIPAAm-grafted layer is that it is reversible-temperature-responsive (Haraguchi *et al*., 2012a). Above 32 °C, the surface is hydrophobic, leading cells attach and proliferate to confluence as monolayer. Below 32 °C, the surface is hydrophilic and the monolayer cell sheet can be easily detached from the surface. Because cell sheets can be harvested by simply changing the temperature without using enzymatic treatment, the cell-cell connections are preserved intact for maintaining better biological function of the cells. Moreover, the accumulated extracellular matrix (ECM) is also maintained around the cells by using this technique. Since ECM can be used as a glue to stack monolayers to make up a 3D multilayered cell sheet, without any scaffold, they are also useful for directly transplanting the cell sheet onto the host tissue without sutures (Haraguchi *et al*., 2012b). Cell sheet technology has been used to fabricate several functional tissue sheets, which treat a wide range of diseases from corneal dysfunction to esophageal cancer, tracheal resection, and cardiac failure (Yang *et al*., 2007).

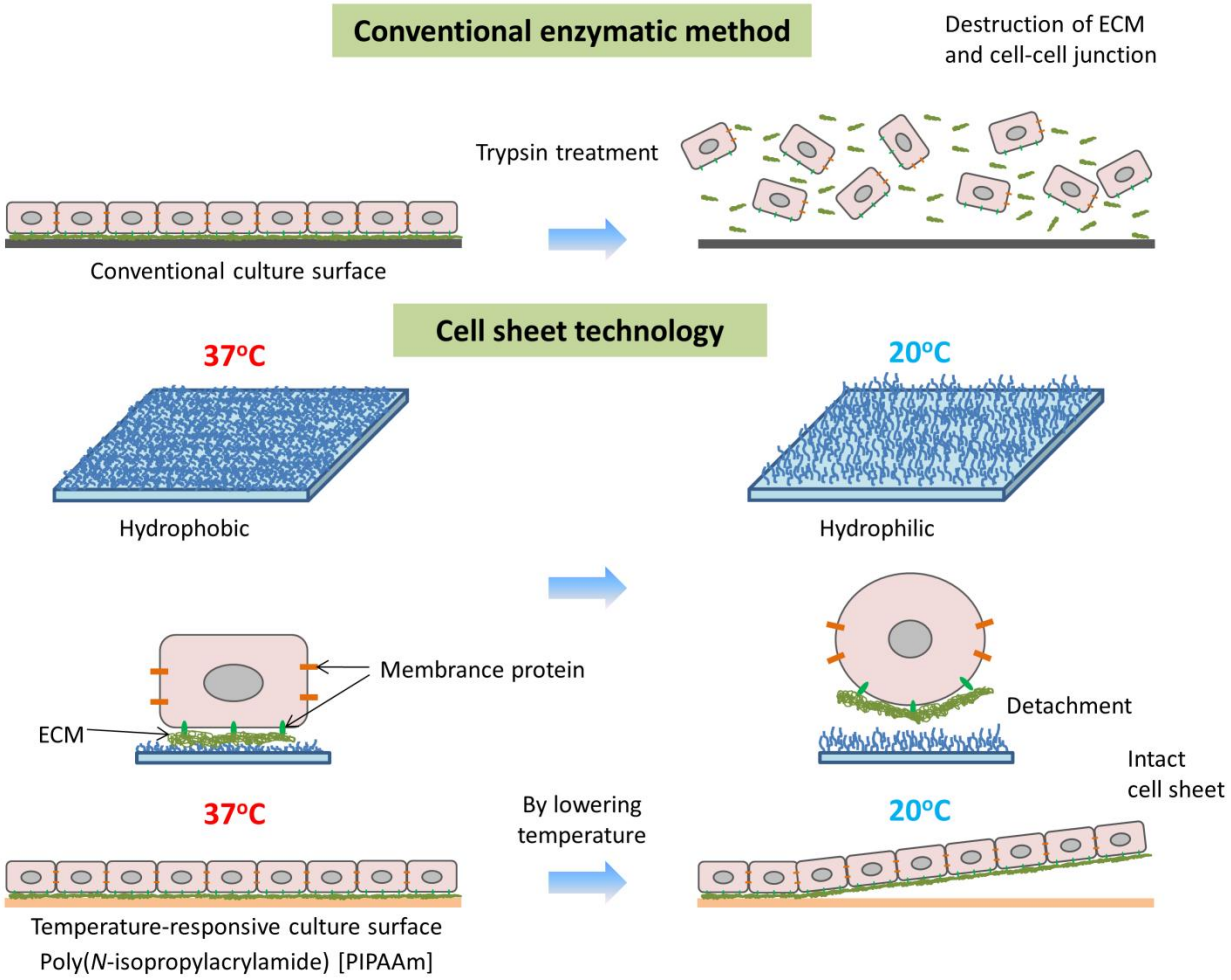

Fig. 1 Cell sheet technology using temperature-responsive culture surface.

Myoblast cell sheet for curing myocardial infarction

Recently, autologous transplantation of multilayered skeletal myoblast sheet is emerging as a new advanced technique for curing myocardial infarction, commonly known as a heart attack, which is associated with the dysfunction of cardiomyocytes and irreversible cell loss caused by the abrupt occlusion of one or more of the blood vessels supplying blood to the heart (Haider *et al*., 2004; Memon *et al*., 2005) (**Fig. 2**). Skeletal myoblast cells are chosen because they are easy to be harvested from patients, have ability to become active, self-renew and differentiate, permitting muscle regeneration upon muscle injury (Jawad *et al*., 2007; Menasche, 2008).

Skeleton myoblast cells also have the ability to contract, as well as being easy to culture, multiply and recognize *in vitro* (Jawad *et al*., 2007). Using this type of cell can also help avoid the ethical debate nowadays. Outstandingly, many researchers have shown the potential of the skeletal myoblast sheet in improving heart functions by its secreting some important cytokines, such as vascular endothelial growth factor (VEGF), hepatocyte growth factor (HGF) and stromal-derived factor 1 (SDF-1), which can promote angiogenesis, i.e., the formation of new capillaries formation from pre-existing ones, and attract the progenitors to come and mend the infarction area (Jawad *et al*., 2007; Memon *et al*., 2005; Perez-Ilzarbe *et al*., 2008; Taylor *et al*., 1998) (**Fig. 2**).

Cell sheet technology has been chosen for autologous transplantation of skeletal myoblasts because it can overcome the limitations of direct injection of myoblast cell suspension to the damaged heart, in which approximately 90 % cells cannot be engrafted (Hata *et al*., 2006; Memon *et al*., 2005; Menasche, 2008; Perez-Ilzarbe *et al*., 2008). Using the temperature-responsive surface, a cell sheet can be harvested with an intact vital cell-cell junctions and extracellular matrix (ECM), which plays the role of a glue in attaching the engineered tissue to the host after transplantation (Jawad *et al*., 2007). Transplantation using cell sheet also overcomes the limitation of conventional cell injection, including the direct needle injury to the already compromised heart. The cell sheet also has the ability to cover a large infarction area, due to the increased survival rate of the transplanted cells (Sekiya *et al*., 2013). Importantly, the transplantation of myoblast sheet could also limit the possibility of early postoperative arrhythmic events (Sawa *et al*., 2012; Sekiya *et al*., 2013), compared with the direct injection of myoblast cell suspensions (Coppen *et al*., 2008). This merit can be attributed to the alignment of the cell sheet myofibers with the host myocardium, which allows the cell sheet to react better in

response to the pulsation of the host myocardium (Sekiya *et al*., 2013). In addition, Sekiya *et al*. reported that the implantation of multilayered myoblast sheets such as three-layered and five-layered sheets yielded favorable results, with better improvements in the cardiac function, the induction of angiogenesis, the presence of more elastic fibers, and less fibrosis compared with that of a monolayer sheet (Sekiya *et al*., 2009).

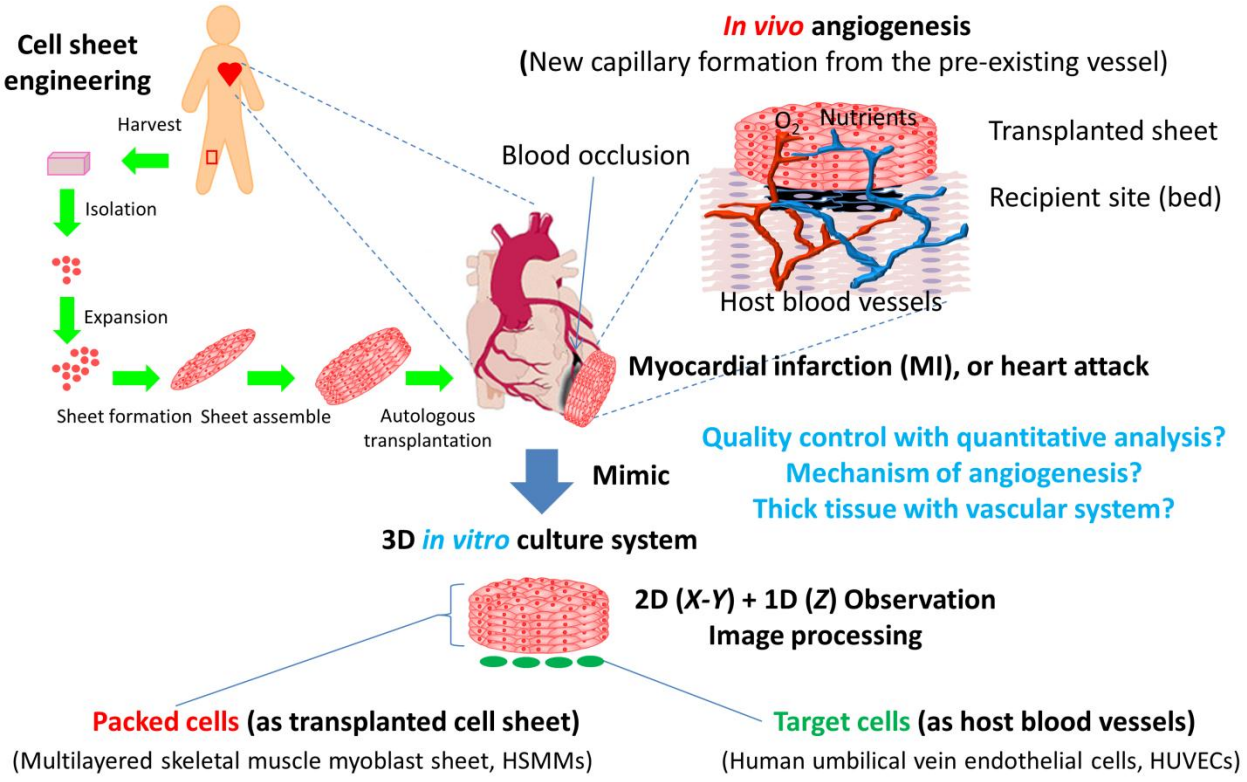

Fig. 2 Autologous transplantation of myoblast cell sheet for curing myocardial infarction.

Necessity of studying the endothelial network formation process inside the multilayered myoblast sheet

From the manufacturing point of view, process and quality control are important for realizing the commercialization of the autologous myoblast sheet transplantation. Obtaining reproducible and well characterized cell therapy products is quite difficult due to the individual

variability between patients. For example, myoblasts from female patients have recently been shown to have a greater proliferation potential than those of male origin (Deasy *et al*., 2007). Population balance of myoblasts compared to fibroblasts during cell expansion, which affects the treatment effect, also depends greatly on age, sex and race of patients, as well as on the *in vitro* culture conditions, including medium and surface coating materials (Kino-oka *et al*., 2013). Experiments using cell culture *in vitro* are one of the promising methods which can evaluate the performance of transplants. To estimate the therapeutic effects of the cell sheet, gene or protein expressions related to cytokine production from the cell sheet were evaluated in previous studies (Memon *et al*., 2005; Perez-Ilzarbe *et al*., 2008). Although such quantitative methods are beneficial for the estimation of the paracrine effect related to angiogenesis, the effects of the cell sheet properties on the dynamic behavior of endothelial cells, including the migration from host to the transplanted myoblast sheets during angiogenesis, remain unclear.

To understand the endothelial behavior inside the 3D cell sheet, the elucidation of tissue dynamics due to myoblast migration inside the sheet is also important. However, spatial cell movement in 3D tissues, especially in the vertical direction, has not been quantitatively investigated due to the absence of methods. Therefore, in this study, using cell sheet technology, the author aimed to construct a novel 3D *in vitro* culture system which is the incubation of multilayered myoblast sheet (packed cells) as transplanted cell sheets and endothelial cells (target cells) as host blood vessels to mimic the *in vivo* angiogenesis post-transplantation (**Fig. 2**). This 3D *in vitro* culture system functioning as a plate shaped aggregate could be observed separately in 2D (*X*-*Y*) and 1D (*Z*) direction. The dynamic behaviors of myoblasts (packed cells) and endothelial cells (target cells) live-stained with different colors in 3D cell sheet were observed and investigated with several image processing methods. The methods developed in

this study, i.e., analysis of sheet thickness, cellular vertical localization, cell migration, length and tip of endothelial network, will be applicable in the quality control of transplants. The results obtained in this research might also offer a deeper understanding of the post-transplantation angiogenesis of the cell sheet, as well as show how the cell sheet integrates functionally with the host.

In addition, the transplantation of myoblast cell sheets is facing a major obstacle of tissue engineering, which is the inability to maintain thick, viable tissue because of the lack of a functional vascular network formation within the engineered tissue (Ko *et al*., 2007). The important question is how many myoblast layers should be stacked and transplanted to obtain the best healing effect, especially for a patient with end-state heart failure. So far, transplantation is limited to only a four-layered sheet (Sawa *et al*., 2012). When more than four grafts were implanted, central necrosis was observed instead of rapidly organized microvasculature, because of the insufficient oxygen supply (Miyagawa *et al*., 2011). To reach a better biological function with a thick myoblast sheet, it is necessary to fabricate a functional vessel network to supply the nutrients and oxygen, as well as to remove the waste products before transplantation. The endothelial network in the cell sheet has the ability to connect to the vessel from the host and improve the survival rate of transplanted tissue (Sekiya *et al*., 2006). One of the proposed methods is a co-culture myoblast sheet with endothelial cells to induce pre-vascularization. The understanding of endothelial network formation in this study is necessary for further success in transplantation.

Outline of the present study

The study of endothelial network formation in multilayered myoblast sheet is important for the understanding of the mechanism by which endothelial cells migrate during the angiogenesis occurring in the cell sheet after the transplantation, toward improving the quality, survival and biological function of engineered tissues (**Fig. 2**). The scope of this study, consisting of three chapters, is shown in **Fig. 3**.

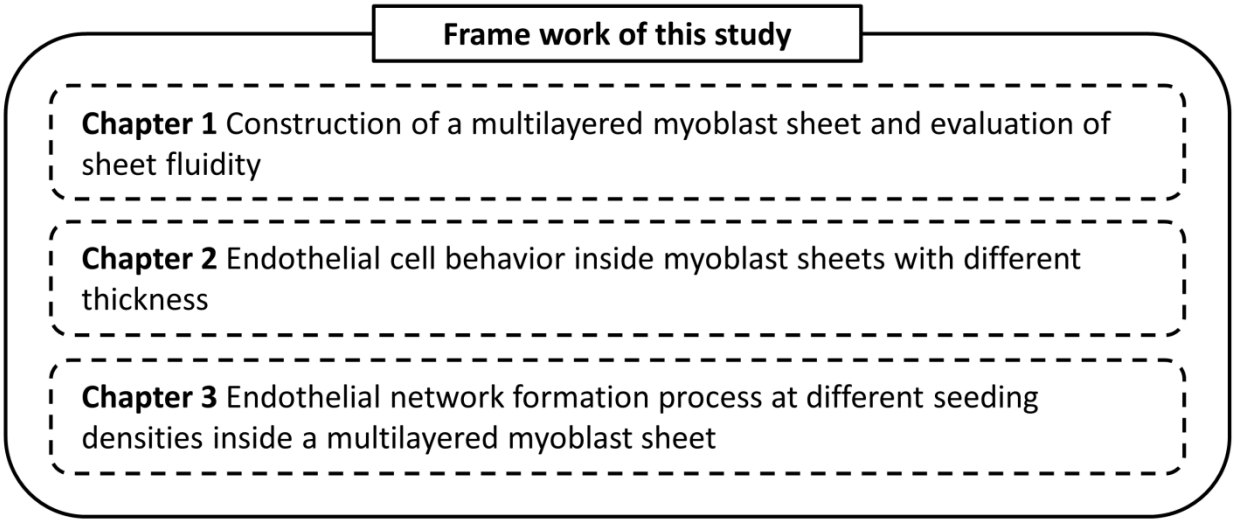

Fig. 3 Outline of study on endothelial network formation in fluidic multilayered myoblast sheet.

Chapter 1 focuses on the fabrication of a multilayered myoblast sheet using a temperature-responsive surface and stamp system. Observation and image processing methods were improved to analyze cell localization in a 3D cell sheet, revealing the migration of human skeletal muscle myoblasts (HSMMs) which acts like a fluidic scaffold. The effect of cellular population balance after the addition of human dermal fibroblasts (HDFs) into the cell sheet on sheet fluidity was investigated.

Chapter 2 describes the construction of a novel 3D *in vitro* culture system, consisting of green fluorescent protein expressing human umbilical vein endothelial cells (GFP-HUVECs)

cultured under HSMM sheets with different layer numbers. The number of the layer in the myoblast sheet was changed to vary its thickness and investigate the effect of cell sheet thickness on endothelial behavior.

Chapter 3 investigates the HUVEC behavior in the multilayered HSMM sheet during network formation process. Image processing was improved to analyze the total length, total tip number and the localization of the endothelial network in the cell sheet. The effect of endothelial seeding density on network formation and vertical localization in the cell sheet was clarified.

Chapter 1

Construction of a multilayered myoblast sheet and evaluation of sheet fluidity

1.1 Introduction

Cell sheet engineering is emerging as an advanced technique for preparing scaffold-free 3-dimensional (3D) tissue (Yang *et al*., 2005), not only for transplantation but also for *in vitro* research. A temperature-responsive poly-*N*-isopropylacrylamide (PIPAAm) grafted surface can be used to form a cell sheet without any enzymatic digestion, thereby which permits to retain an intact extracellular matrix (ECM) (Yang *et al*., 2005). Sasagawa *et al.* previously constructed a multilayered structure of skeletal muscle myoblast cells in which prevascular formation by endothelial migration was observed (Sasagawa *et al*., 2010).

Cell migration in a 3D construct plays an important role in physiological and pathological phenomena such as embryonic development, cell alignment, immune reaction, angiogenesis, and metastasis (Horwitz and Webb, 2003a). The understanding of the mechanisms of cell migration will be useful in the design of biomimetic structures and functional engineered tissues. Although the behaviors of cells on 2D culture surfaces have been extensively investigated (Bondesen *et al*., 2007; Chowdhury *et al*., 2009; Louis *et al*., 2008; Wang *et al*., 2009), spatial cell movement in 3D tissues, especially with regard to vertical migration inside the tissue, has not been investigated due to the absence of methods to allow *in vitro* quantitative and reproducible measurements. In Chapter 1, a five-layered HSMM sheet was fabricated as a 3D model using temperature-responsive surface and stamp system. HSMMs as packed cells were live-stained to evaluate vertical cell migration by confocal laser scanning microscopy and image processing.

1.2 Materials and methods

1.2.1 Cell culture

HSMMs (Lot. No. 4F1618; Lonza Walkersville Inc., Walkersville, MD, USA) and HDFs (Lot. No. 6F4296; Lonza Walkersville Inc.) were used in the experiments. According to procedures described elsewhere (Chowdhury *et al*., 2009; Chowdhury *et al*., 2010), subculture of HSMMs on laminin-coated surface was carried out at 37 °C in an atmosphere of 5% CO_2 in Dulbecco's modified Eagle's medium (DMEM; Sigma-Aldrich, St. Louis, MO, USA) containing 10% (v/v) fetal bovine serum (FBS; Invitrogen, Grand Island, NY, USA) and antibiotics (100 U/cm^3 penicillin G, 0.1 mg/cm^3 streptomycin, and 0.25 mg/cm^3 amphotericin B; Invitrogen). Subculture of HDFs also used the same conditions as subculture of HSMMs, but on normal culture surface without laminin coating.

1.2.2 Fabrication of multilayered cell sheet using stamping method

As shown in **Fig. 1.1A**, starter cells harvested from the subcultures were stained using CellTracker Green^{TM} and CellTracker Orange^{TM} (Invitrogen) to exhibit fluorescently green and orange cells, respectively, according to commercially recommended protocol (5 μM for 15 min for live cell imaging). The stained cells were employed in the fabrication of the multilayered sheet according to newly developed procedures as follows. HSMMs were seeded at 2.3×10^5 cells/cm^2 in each well (diameter, 1.9 cm^2) of 24-well UpCell^{TM} plates (CellSeed, Tokyo, Japan) with a temperature-responsive surface grafted with PIPAAm and incubated for 24 h at 37 °C in 5% CO_2 to form the monolayer sheet. The medium depth was set to 2 mm throughout the experiments and HDFs were mixed into the sheet if needed. For stacking monolayer cell sheets to form the

multilayered cell sheet, a manipulator was designed as shown in **Fig. 1.1B** composed of a stamp, its stand, and a mold to load the stamp with the gelatin gel. A solution of 7.4% (v/v) gelatin was prepared by dissolving gelatin powder (G1890-100G; Sigma-Aldrich) in 5 mL Hank's balance salt solution (Sigma-Aldrich) and 100 μL of 1N NaOH solution at 45 °C for 30 min. The solution was then sterilized by filtration through a 0.22-μm filter (Millex-GS; Millipore Co., Billerica, MA, USA) and poured into the silicone molds under aseptic conditions. The stamps were put onto the molds on ice to gelation. Finally, the molds were gently removed and the stamps with the gelatin were ready to be used to stack the cell sheets. To harvest the monolayer sheet, the stamp with the gelatin gel was overlaid on the monolayer sheet in a well at 37 °C and the temperature was shifted to 20 °C (**Fig. 1.1A**). After 30 min, the stamp was lifted together with the monolayer sheet from the bottom surface of the well. The steps were then repeated for the sequential harvests of monolayer sheets to form the multilayer structure on the stamp. The multilayered sheet with the gelatin was separated from the stamp and placed on a 35-mm culture dish (ibidi GmbH, Martinsried, Germany) that was precoated with 0.2 mL/cm^2 FBS for 24 h for the facilitation of the sheet attachment to the surface, and the dish was incubated for 2 h at 20 °C in 5% CO_2 without the addition of medium. To remove gelatin, the medium (0.4 mL/cm^2) was added, and the temperature was shifted to 37 °C for 1 h to melt the gelatin and the medium was changed with fresh one. In the present study, the fabricated culture system of a five-layered sheet was used to analyze cell behaviors.

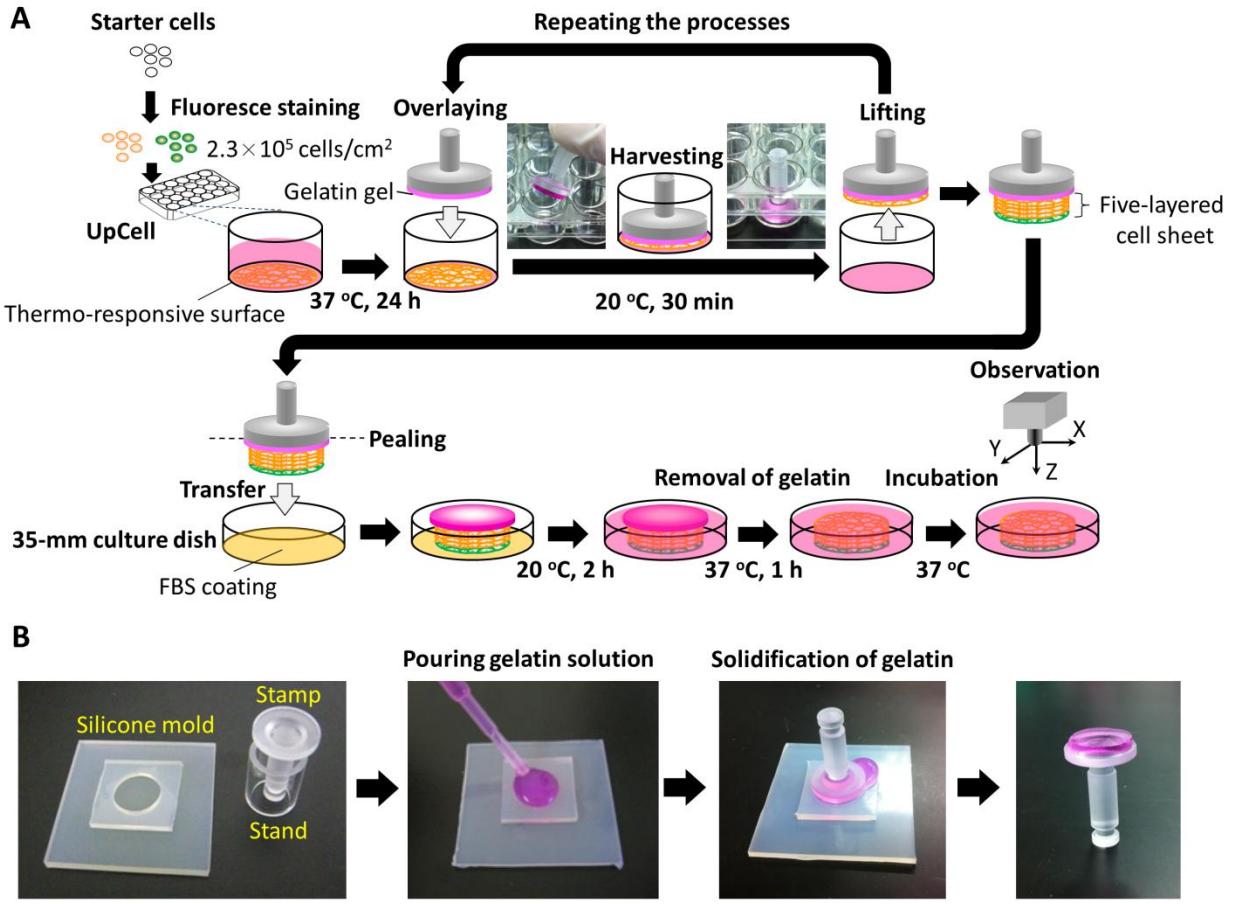

Fig. 1.1 Schematic diagrams showing the fabrication of a multilayered cell sheet. (A) Procedure of preparing monolayer sheet and stacking method using gelatin stamp. (B) Preparation of the manipulator used to harvest the cell sheet.

1.2.3 Stereoscopic observation

As a typical culture system, the five-layered sheet consisting of basal layers (green) as target cells and other layers (orange) as packed cells stained by CellTracker Green™ and CellTracker Orange™, respectively, was prepared for the observation of tempo-spatial cell distribution using confocal laser scanning microscopes (FV10i for time lapse and FV-300 for spatial distribution; Olympus, Tokyo, Japan) with 10× and 60× objective lens. To determine the

spatial distribution of the target cells, the green and orange cells in each layer at 0 and 48 h of incubation were observed and quantitatively analyzed using image processing. The five-layered sheet was washed twice with phosphate buffered saline (PBS) and then fixed with 4% paraformaldehyde in PBS (Wako Pure Chemical Industries, Osaka, Japan) overnight. After washing with PBS, at least eight random positions of each sample were scanned at a 0.6-μm interval to yield slice images for vertical direction determination.

To estimate the cell migration rate in 2D surface, the dynamic of individual myoblast and dermal fibroblast were observed using an image capturing tool and calculated as described elsewhere (Chowdhury *et al*., 2009; Kino-oka *et al*., 2004).

1.2.4 Image processing to analyze cell spatial distribution and diffusivity

After intensity threshold values were identified, 8-bit images (256 × 256 pixels) of both colors in each slice were converted into binary images, leading to the distinction between colored and non colored pixels. Here the colored pixels which were derived from green and orange fluorescent original images denoted the green and orange pixels, respectively (**Fig. 1.2**). The number of colored pixels in each slice was counted. The green and orange pixels in each slice were normalized using the maximum green and orange pixel values, respectively, found in all of the slice images. The slice possessing more than 10% of the colored pixels was regarded to exist inside cell sheet, from which the vertical positions at top and bottom of the five-layered sheet, and the sheet thickness, *h*, were determined. The ratio of green pixels to sum of green and orange pixels in each slice was normalized to determine the distribution of green pixels by dividing into 5 layers. Here, the normalized distribution of green pixels was assumed to be equivalent to the green cell distribution in the sheet, recorded by the frequency of green cells, f_G (-), in each layer.

To quantitatively analyze vertical sheet fluidity, the diffusivity, D, was determined based on Fick's second law, $\frac{\partial f_G}{\partial t} = D\frac{\partial^2 f_G}{\partial h^2}$, in which f_G, t, and h represent the green cell frequency, incubation time, and sheet thickness, respectively. The Crank-Nicolson finite difference method and least squares method were applied to calculate the diffusivity using a custom-made software programmed by LabVIEW (National Instruments, Austin, TX, USA). The initial condition was that the total ratio of green cells in the five layers was normalized to 1. The free boundary condition, $\frac{df_G}{dh} = 0$, is set at both the bottom and the top of the five-layered sheet.

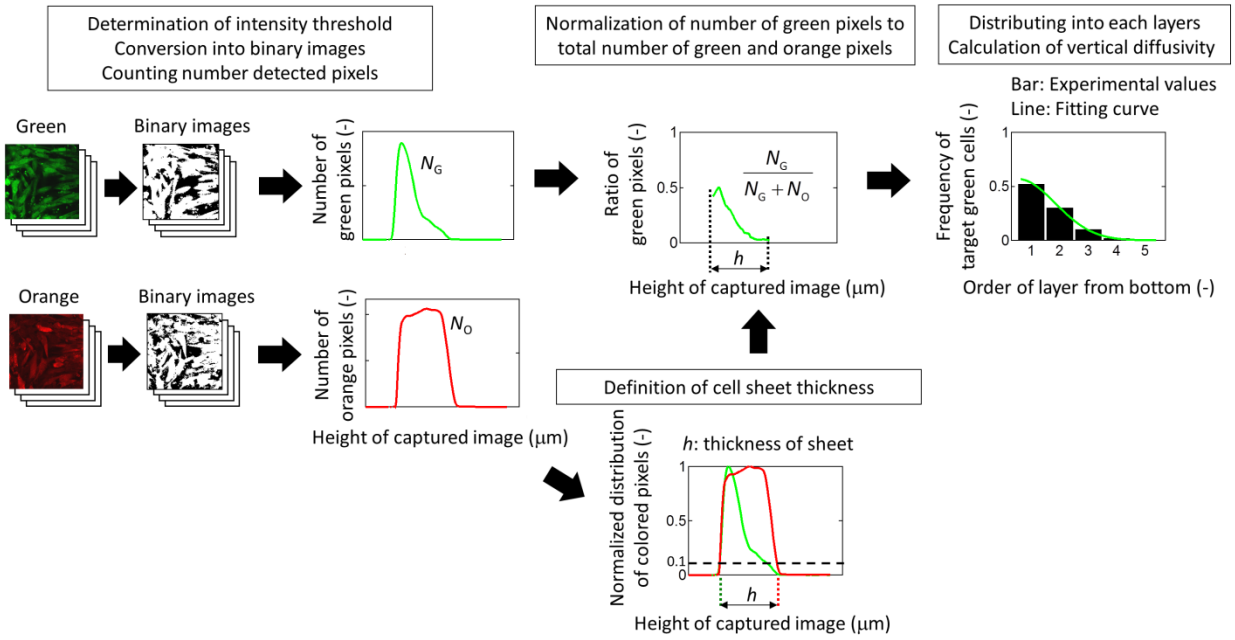

Fig. 1.2 Image processing system calculating the spatial distribution and diffusivity of the green target cells.

1.3 Results

1.3.1 Cell migration inside 3D cell sheet making sheet fluidity

Time-course observation was conducted to observe localization of green target cells at 0 and 48 h inside five-layered sheet. At t = 0 of incubation, the green cells were observed in the bottom of the sheet (**Fig. 1.3A**). However at t = 48 h, the green cells were observed in upper layers of the cell sheet (**Fig. 1.3B**), indicating the active cellular migration occurred in the horizontal and vertical directions anywhere in the sheet, revealing the sheet fluidity.

To understand the extent of the sheet fluidity, the vertical distribution of green cells was estimated. **Fig. 1.3C and D** shows the histograms of f_G at 0 and 48 h, respectively. At t = 0, the f_G values in the first and second layers from the bottom surface were estimated to be f_G = 0.82 and 0.17, respectively, and the sheet at t = 48 h had a broad distribution of f_G, being f_G = 0.37 in the first layer. In addition, the f_G decreased gradually along the layers from bottom to top, suggesting the analogy of vertical migration to molecular diffusion. To quantitatively analyze vertical sheet fluidity, the diffusivity, D, was determined (**Fig. 1.2**). In a practical aspect, the f_G distribution data at 0 and 48 h were applied to calculate the apparent vertical diffusivity of green target cells from overall bottom layer, $\overline{D}_O$, being $\overline{D}_O$ = 0.74 μm^2/h (**Table 1.1**).

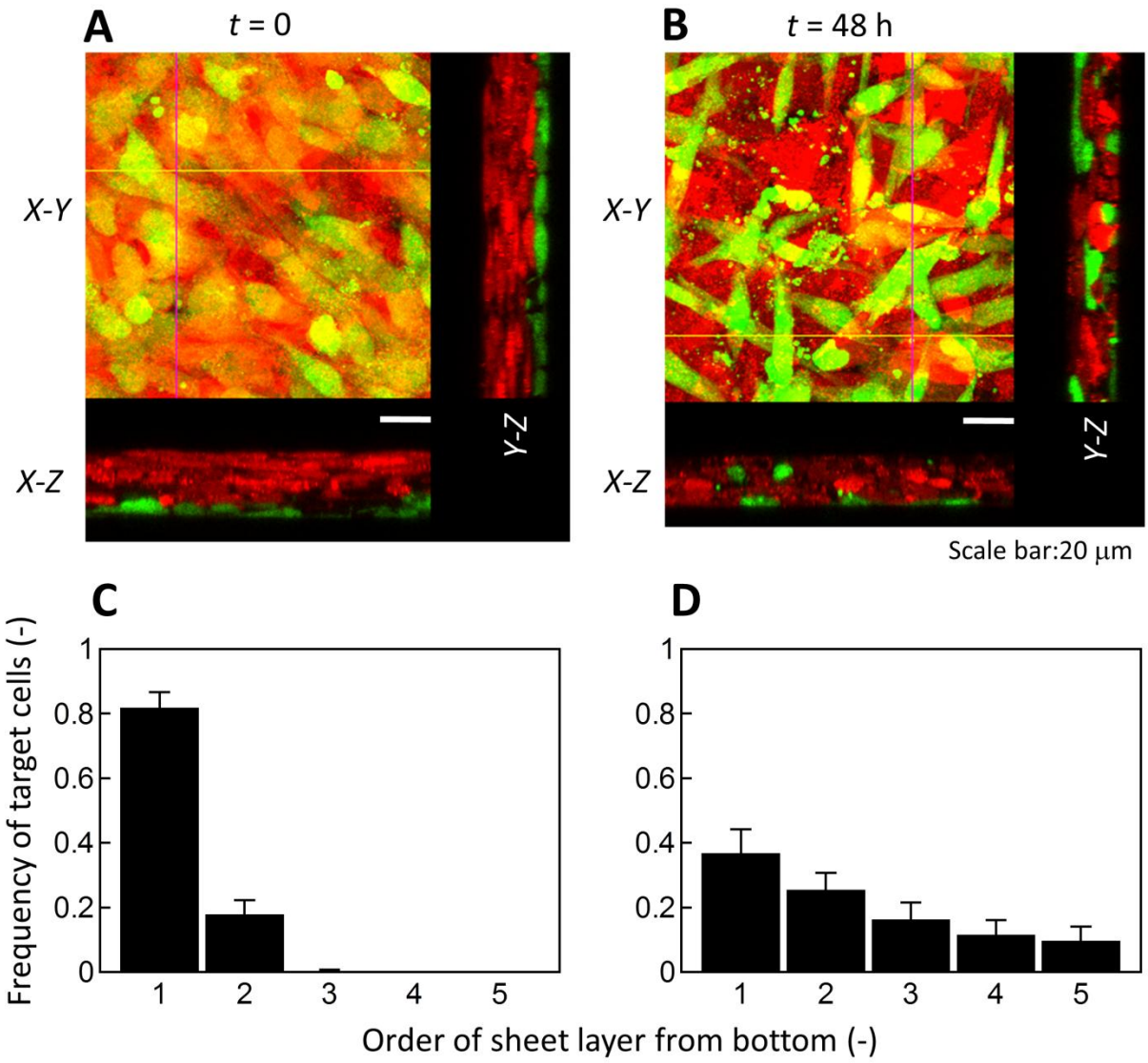

Fig. 1.3 Cell migration inside 3D cell sheet making sheet fluidity. Representative images showing different localizations of green target cells at t = 0 (A) and t = 48 h (B), indicating cell migration from bottom layer to upper layers. The *X*-*Y* stacked images were constructed from the *X*-*Y* images at 0.6-μm intervals. The *X*-*Z* and *Y*-*Z* images were constructed along with the yellow and pink lines drawn in the *X*-*Y* stacked images, respectively. Scale bar: 20 μm. Spatial distributions of the green target cells inside the cell sheet at t = 0 (C) and t = 48 h (D). Bars show the standard deviation (SD) (n = 3).

To have deeper understanding on this phenomenon, vertical migration of green target cells from top layer was observed and analyzed. Green cells, which were initially on the top layer at t = 0 (**Fig. 1.4A**), migrated into middle and basal layers at t = 48 h (**Fig. 1.4B**). The spatial distribution of target cells from top layer at t = 0 and t = 48 h (**Fig. 1.4C and D**) were reverse of that of from basal layer (**Fig. 1.3C and D**). The diffusivity of green target cells from overall top layer, $\bar{D}_O$, was 0.76 μm^2/h, a little higher than that of basal layer, but the difference was insignificant ($p < 0.05$). The similar diffusivity of cells from bottom and top layer indicated that cells migrated freely inside the cell sheet with the same manner, making sheet fluidity.

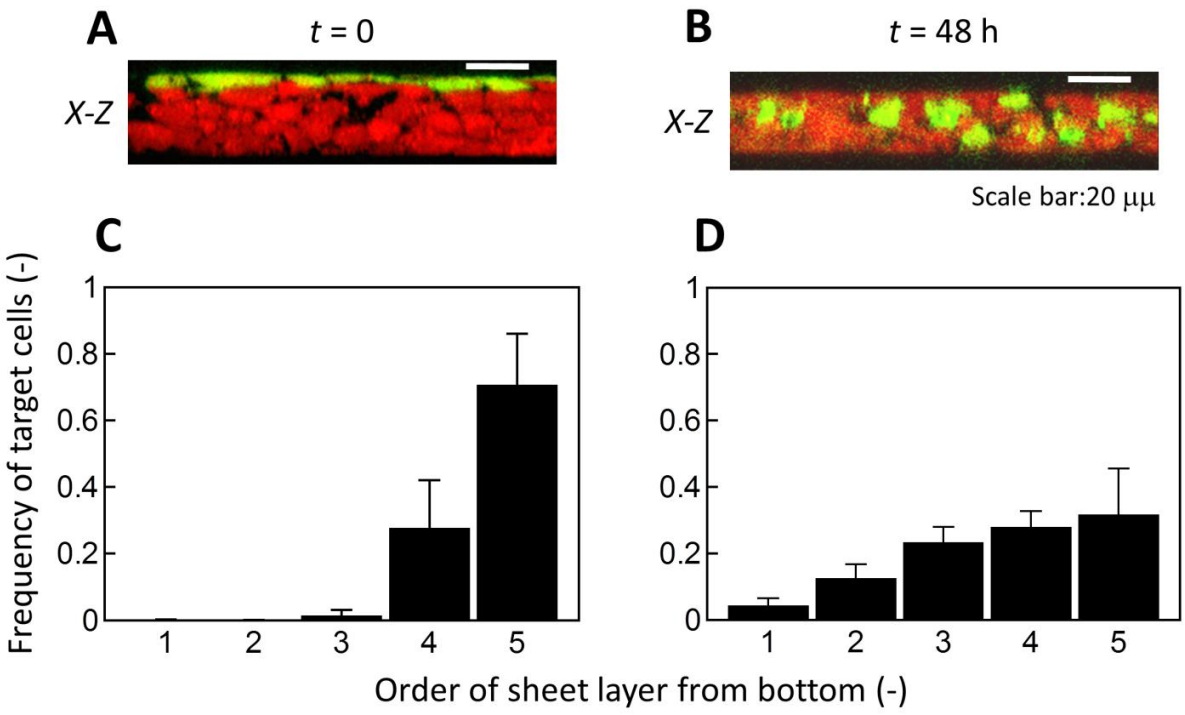

Fig. 1.4 Cell migration from the top layer of 3D cell sheet. Representative images showing different localizations of green target cells from top layer at t = 0 (A) and t = 48 h (B), indicating cell migration from top layer to middle and bottom layers. Scale bar: 20 μm. Spatial distributions of the green target cells inside the cell sheet at t = 0 (C) and t = 48 h (D). Bars show the SD (n = 3).

Table 1.1 Diffusivities of different target cells from the basal layer in the five-layered cell sheet at different cellular population balance conditions.

Condition	HSMMs (%)	HDFs (%)	Sheet thickness at initial, h (μm)	Diffusivity (μm^2/h)		
				$\overline{D}_{\mathrm{O}}$	$\overline{D}_{\mathrm{M}}$	$\overline{D}_{\mathrm{F}}$
A	100	0	33.0 ± 5.4	0.74 ± 0.23	-	-
B	75	25	36.4 ± 5.4	1.57 ± 0.50	0.57 ± 0.14	2.40 ± 0.49
C	50	50	37.7 ± 5.0	0.69 ± 0.12	0.54 ± 0.26	0.80 ± 0.36

$\overline{D}_{\mathrm{O}}$, $\overline{D}_{\mathrm{M}}$, $\overline{D}_{\mathrm{F}}$ are the diffusivities of overall basal layer, HSMMs, and HDFs from the basal layer, respectively.

All values are mean ± SD (n = 3).

1.3.2 Effect of dermal fibroblast addition on sheet fluidity

To investigate variation of sheet fluidity, we incubated five-layered sheets added with HDFs comprising 25% and 50% of the cell counts as conditions B and C, respectively (**Table 1.1**). As shown in **Table 1.1**, the $\overline{D}_{\mathrm{O}}$ increased 2.1 times at 25% addition (condition B) compared to that without any HDF addition (condition A), although the significance level was not sufficient (p < 0.06). In addition, the $\overline{D}_{\mathrm{O}}$ decreased 2.3 times at 50% addition (condition C) compared to that at 25% addition (p < 0.05).

For further understanding of the role of HDFs addition, the author established the five-layered sheet system composed of HSMMs or HDFs in basal layer stained by CellTracker Green$^{\mathrm{TM}}$ and the rest of cells stained by CellTracker Orange$^{\mathrm{TM}}$ and estimated the diffusivity of basal HSMMs or HDFs, $\overline{D}_{\mathrm{M}}$ or $\overline{D}_{\mathrm{F}}$, respectively (**Table 1.1**). At 25% addition, $\overline{D}_{\mathrm{F}}$ was estimated

to be 2.40 μm^2/h, being 4 times larger than $\bar{D}_{\mathrm{M}}$. An independent experiment showed that the migration rate of single HDFs is 1.5 times higher than that of single HSMMs in 2D culture using a conventional T-flask (**Fig. 1.5**). At 50% addition, $\bar{D}_{\mathrm{F}}$ decreased 3 times to 0.80 μm^2/h, although $\bar{D}_{\mathrm{M}}$ stayed almost constant, to be 0.54 μm^2/h, suggesting that $\bar{D}_{\mathrm{O}}$ depended on HDF migration in the sheet.

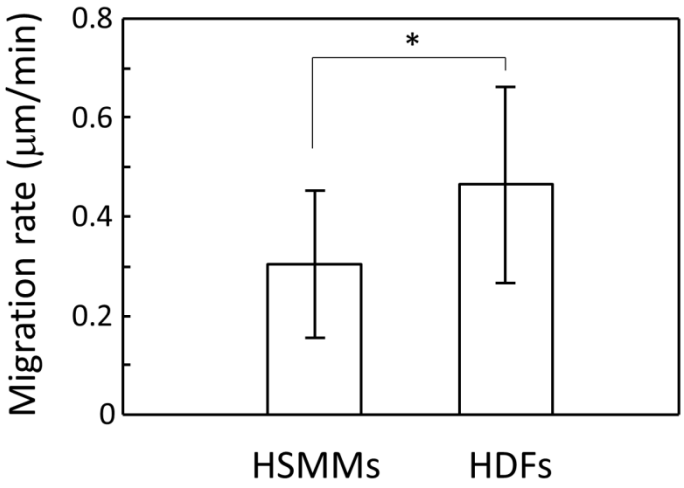

Fig. 1.5 Migration rate of single myoblasts and fibroblasts in low density 2D culture. The bars show the SD (n > 20). The asterisk shows significant difference ($p < 0.02$).

1.4 Discussion

Understanding of myoblast behavior is the prerequisite to access further success in transplantation of multilayer cell sheet for curing myocardial infarction. Despite their behaviors on 2D culture surface have been investigated extensively, understanding on behavior of myoblasts in 3D models - having better represent to microenvironment of living tissues - remains a challenge. In this study, the author has designed five-layered myoblast sheet as a 3D model to understand cell migration of packed cells with quantitative analysis by image processing. It was found that myoblasts actively migrated both in horizontal and vertical directions inside the cell

sheet causing sheet fluidity (**Figs. 1.3 and 1.4**). The vertical cell localization and migration were quantitatively analyzed by using frequency of target cells in each layers and diffusivity, respectively. HDFs were found to affect strongly the migration of the cell sheet.

The inner structural fluidity of cells in 3D constructs has been reported in cultured neurospheres (Singec *et al*., 2006) and embryoid bodies (Dang *et al*., 2002). In static suspension cultures of mouse neural stem cells, active migration of single cells caused aggregate formation through intercellular coalescence, and culture prolongation led to cell division in the aggregates as well as accidental coalescence between independent aggregates that formed large spheres in which the location of distribution of differentiated neurons and glia was observed (Mori *et al*., 2007). Further observation revealed that the large sphere was caused by spontaneous active migration in aggregates through the live-cell imaging technique. In addition, Duguay *et al*. reported that aggregation using a mixture of E-cad–expressing E8a cell line and P-cad–expressing LP1 cell line caused spatial habitat isolation of 3D spheres via active cell migration and intercellular binding affinity, leading to autonomous double-layer spheres by different cell types (Duguay *et al*., 2003). These results mean the importance of cell migration in 3D constructs affecting the fate of stem cells as well as spatial habitat isolation of differentiated cells. In the current study, HDF addition was found to affect sheet fluidity. Pittet *et al.* reported that HDFs exhibited strong OB-cadherin connection in high-density culture (Pittet *et al*., 2008). These results suggest that HDF active migration physically facilitated the overall fluidity in the sheet at 25% HDF addition levels. It is most likely that 50% HDF addition induced strong HDF intracellular bindings in the sheet, and this strong interaction with lower HDF migration rates resulted in the decline of overall sheet fluidity. Further experiments clarified the localization of HDFs in five-layered sheets (Oda, M. *et al*., Abstr., 10th Congress of the Japanese Society for

Regenerative Medicine, p. 248, 2011). This finding suggested that the cell sheet fabricated from HMMs and HDFs exhibited the habitat isolation between them.

Many researchers have paid much attention to tissue mimicry by using cellular aggregates, which are considered minimized functional structures. The mimic constructs have broad potential use as transplants in regenerative medicine as well as structural material for elucidating the dynamic tissue development mechanism. From the standpoint of analytical techniques, observational convenience of 3D constructs is a critical requirement because cellular behaviors such as migration, division, and communication affect the common mechanisms of tissue development.

In conventional studies, most of the techniques for fabricating cell aggregates led to spherically shaped constructs through spontaneous formation by cellular coagulation. In contrast, the current system applied the plate shape of the multilayered sheet using artificially designed formation by the assembly of monolayer sheets because the mimic system using the plate-shaped aggregate has the observational advantage in the 3D construct. The plate-shaped aggregates can be fabricated in various ways using cell sheet engineering technique with temperature-responsive polymer grafted surface (Yang *et al*., 2005), biodegradable peptide grafted surface (Qiu *et al*., 2010) or collagenase degradable atelocollagen film (Nagai *et al*., 2004), magnetic-force based tissue engineering technique (Ito *et al*., 2005), layer-by-layer assembly technique with ECM coating cells (Matsusaki *et al*., 2007), compressed collagen sheet (Brown *et al*., 2005), vitrified collagen film “vitrigel” (Takezawa *et al*., 2007), and bioprinting method (Nakamura *et al*., 2010).

In this study, the system that uses multilayered cell sheet containing stained target cells in the basal layer and confocal laser scanning microscopy realizes clear observation of target cell behaviors in the vertical direction, enabling monodimensional analysis of vertical cell

distribution inside the sheet. The reduced spatial dimension makes it easy to analyze cell migration, compared to the full 3D analysis required of spherically shaped aggregates. Thus, the system developed in the present study can be a powerful tool for elucidating dynamic phenomena in 3D constructs.

1.5 Summary

The procedure for fabricating a multilayered cell sheet was developed by using cell sheet technology. The target cells and packed cells were live-stained with different colors, and seeded at high density onto a temperature-responsive culture surface, to form a monolayer cell sheet after 24 h of incubation. The monolayer cell sheets were detached simply by lowering the temperature of the culture surface to 20 °C, and stacked together to form a multilayered cell sheet using a customized stamp system with gelatin. Confocal laser scanning microscopy revealed the dynamic migration of myoblasts inside cell sheet to be sheet fluidity. Image processing was improved to evaluate the vertical spatial distribution of target cells, indicating the vertical migration of cells during 48 h of incubation, similar to molecular diffusion. Parameter diffusivity was estimated to show the effect of HDF addition on sheet fluidity. This 3D fluidic scaffold was used in the following chapters to construct a 3D *in vitro* culture system used for understanding the endothelial behavior during network formation process.

Chapter 2

Endothelial cell behavior inside myoblast sheets with different thickness

2.1 Introduction

The autologous transplantation of myoblast cells is emerging as a promising technique for treating myocardial infarction, which is associated with cardiomyocyte dysfunction and irreversible cell loss (Memon *et al*., 2005; Miyagawa *et al*., 2011). Skeletal muscle myoblasts were chosen because they are easy to harvest from patients, are easily cultured, multiply *in vitro* (Hassink *et al*., 2003), and can undergo self-renewal and differentiation to heal muscle injury *in vivo* (Al Attar *et al*., 2002). In addition, it has been revealed that myoblasts can secrete some important cytokines such as vascular endothelial growth factor (VEGF), hepatocyte growth factor (HGF) and stromal-derived factor 1 (SDF-1), which improve heart function via the facilitation of angiogenesis and attraction of progenitors to the infarcted area (Memon *et al*., 2005; Perez-Ilzarbe *et al*., 2008). However, Menasche *et al*. reported the possibility of early postoperative arrhythmic events after myoblast transplantation when myoblast cell suspensions were directly injected into the damaged heart (Menasch *et al*., 2008). To overcome this disadvantage, Sawa *et al*. conducted the first clinical trial of myoblast sheet transplantation, which was shown to improve the function of the damaged heart *in vivo* without producing arrhythmic heart beats (Sawa *et al*.). Moreover, it was reported that multilayered myoblast sheets yielded better results, with the improvement in cardiac function, induction of angiogenesis, presence of more elastic fibers, and less fibrosis compared with that of a monolayer sheet (Sekiya *et al*., 2009).

The development of a 3D *in vitro* culture system for endothelial migration is critical in order to elucidate the mechanism by which endothelial cells of the host migrate into the transplanted myoblast sheets. In Chapter 1, a five-layered HSMM sheet was fabricated to evaluate myoblast vertical migration as sheet fluidity by using confocal laser scanning microscope with image processing. In this Chapter 2, using a cell sheet stacking method with newly developed jigs, a novel 3D *in vitro* culture system of multilayered HSMM sheets (packed cells) with green fluorescent protein expressing human umbilical vein endothelial cells (GFP-HUVECs) (target cells) was constructed and the dynamic behavior of endothelial cells was observed inside HSMM sheets with different thickness by varying the layer number of the cell sheet.

2.2 Materials and methods

2.2.1 Cell culture

HSMMs (Lot No. 4F1618; Lonza Walkersville Inc., MD, USA) and GFP-HUVECs (Lot No. 20100201001, Angio-Proteomie, MA, USA) were used in the experiments. According to procedures described elsewhere (Chowdhury *et al*., 2010), subcultures of HSMMs on laminin-coated surfaces were performed at 37 °C in an atmosphere of 5% CO_2 in Dulbecco's Modified Eagle's Medium (DMEM; Sigma-Aldrich, St. Louis, MO, USA) containing 10% (v/v) fetal bovine serum (FBS; Thermo Scientific Hyclone, Logan, UT, USA) and antibiotics (100 U/ml penicillin G, 0.1 mg/ml streptomycin, and 0.25 mg/ml amphotericin B; Invitrogen, Grand Island, NY, USA). GFP-HUVECs were cultured in a commercially available medium (EGM-2; Lonza

Walkersville Inc.). The medium depth was set to 2 mm and renewed every two days throughout the experiments.

2.2.2 Incubation of HSMM sheets with GFP-HUVECs

Monolayer, three-layered, five-layered, and seven-layered HSMM sheets (packed cells) were fabricated using the cell sheet stacking method with newly developed jigs (**Fig. 2.1**), which enable consistency of operation. The HSMMs harvested from the subcultures were stained using CellTracker Orange^{TM} (Invitrogen) to obtain fluorescently orange cells according to a commercially recommended protocol. The HSMMs were seeded at 3.5×10^5 cells/cm^2 in each well of a temperature-responsive 24-well UpCell™ plate (CellSeed, Tokyo, Japan). The wells were mounted in advance with Teflon rings to improve the detachment of the cell sheet in the harvesting operation, as described below. The final culture area in each well was 0.95 cm^2. The seeded cells were incubated for 24 h at 37 °C in a 5% CO_2 atmosphere to form the monolayer sheet. In order to fabricate the gelatin stamp used for stacking the cell sheets, a set of manipulators were prepared with jigs of a holder, metal stamps, a mold, a plunger, and a silicone rubber, thus allowing consistent preparation and handling (**Fig. 2.1A**). A solution of 7.4% (w/v) sterilized gelatin (G1890-100G; Sigma-Aldrich) was poured into the mold, which was mounted on the silicone rubber in advance. The metal stamps on the holder were mounted onto the gelatin and the entire setup was kept at 4 °C for 40 min to solidify the gelatin. After peeling away the silicone rubber, the mold was mounted onto the plunger to collect the gelatin stamps. To harvest the monolayer cell sheet, the stamp with the gelatin was put on the monolayer cell sheet in a well at 37 °C, and the temperature was lowered to 20 °C. The metal stamp has a plate on the top, which fits to the well of the UpCell™ plate to support cell sheet harvesting onto the center of the gelatin gel. After 30 min, the stamp with the harvested cell sheet was lifted from the bottom

surface of the well. The steps were then repeated for sequential harvests of the monolayer cell sheets to form the multilayered cell sheet on the stamp (**Fig. 2.1B**). Using the plastic cap, the multilayered cell sheet was transferred to the center of a 35-mm culture dish (ibidi GmbH, Martinsried, Germany) that contained GFP-HUVECs (target cells) seeded at 0.5×10^4 cells/cm^2 in EGM-2 supplemented with 20% (v/v) FBS and incubated at 37 °C in a 5% CO_2 atmosphere for 24 h in advance. After incubation at 20 °C for 2 h, the cell sheet was incubated at 37 °C in the above-mentioned DMEM containing 10% (v/v) FBS for 1 h to remove the gelatin. The medium containing the dissolved gelatin was replaced with fresh medium. The medium was renewed every day. In the control, GFP-HUVECs were seeded at 0.5×10^4 cells/cm^2 and incubated without overlaying any HSMM sheets under the same conditions as described above.

2.2.3 Observation of GFP-HUVEC behavior

Live-cell imaging was performed at t = 0, 48 and 96 h of incubation to elucidate the morphology of GFP-HUVECs both inside and outside of the cell sheet by using a fluorescence microscope (IN Cell Analyzer 2000, GE Healthcare, Cardiff, UK) with a 10× objective lens. The number of HUVECs attached outside of the cell sheet was manually counted to evaluate cell density. At 0 h and 96 h of cultivation, samples were fixed with 4% (v/v) paraformaldehyde in phosphate-buffered saline (Wako Pure Chemical Industries) overnight. Then samples were observed by using a confocal laser scanning microscope (FV10i or FV1000, Olympus, Tokyo) with a 60× objective lens at 0.6-μm interval for the *z*-axis to understand HUVEC localization in the cell sheet. Image processing for measuring the thickness of the HSMM sheet at t = 0 was performed as described previously in Chapter 1 (**Fig. 1.2**) (Kino-oka *et al*., 2012). Time-lapse live imaging was conducted to understand the dynamic behavior of HUVECs by using a time-lapse confocal laser scanning microscope (FV10i, Olympus) with a 60× objective lens at 0.6-μm

interval for the *z*-axis every 1 h for 20 h of each incubation day. Obtained images were processed using FluoView software (Olympus).

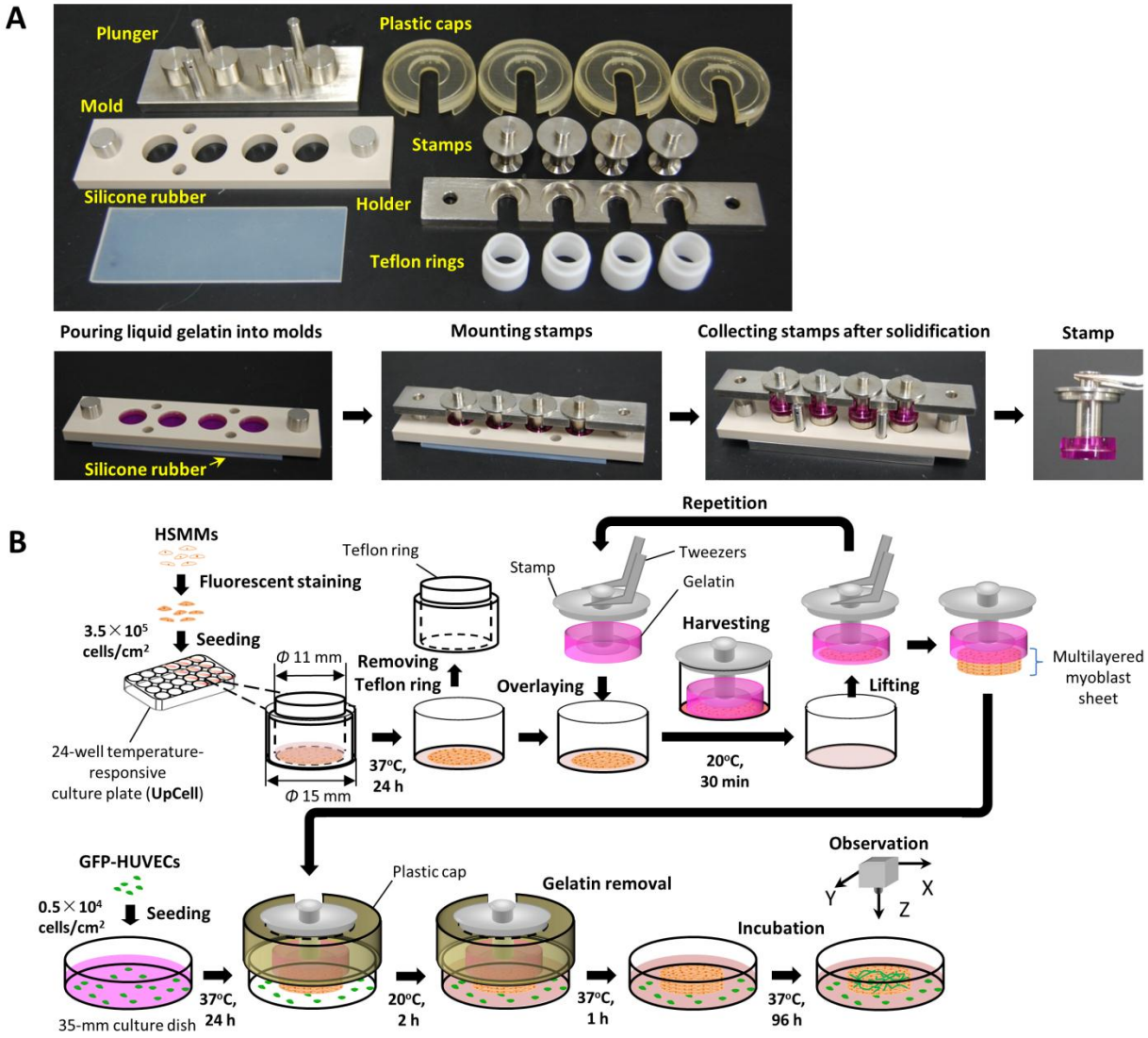

Fig. 2.1 Preparation of 3D *in vitro* culture system of HSMM sheets and GFP-HUVECs using the cell sheet stacking method with newly developed jigs. (A) Components used to make the cell sheets (top panel) and steps used to prepare the stamp with gelatin (bottom panel). (B) An illustration of the procedure for stacking multilayered HSMM sheets and incubating them with GFP-HUVECs.

2.3 Results

2.3.1 Effect of the HSMM sheet thickness on HUVEC behavior

To understand the effect of the HSMM sheet thickness on endothelial behavior, the GFP-HUVECs were incubated under the HSMM sheets with different layer numbers, or without an HSMM sheet as a control. As shown in **Table 2.1**, the initial thickness of the HSMM sheet varied according to the layer number. The thickness of the monolayer HSMM sheet was 16 μm. The three-, five- and seven-layered HSMM sheets were 1.7, 2.4, and 3.5 times thicker than that of the monolayer, respectively. At the onset of incubation (incubation time, t = 0), most HUVECs were single cells under all conditions (**Fig. 2.2A-E**). In the control, the number of HUVECs slightly decreased at t = 48 h, and most HUVECs were detached from the culture surface at t = 96 h (**Fig. 2.2F, K**), indicating the low adhesion and proliferation of HUVECs in DMEM containing 10% (v/v) FBS. In the monolayer HSMM sheet, the number of HUVECs was extremely decreased at t = 48 h and t = 96 h (**Fig. 2.2G, L**) compared with that at t = 0. In the three-layered HSMM sheet, HUVECs formed small island-shaped aggregates at t = 48 h that became much larger at t = 96 h (**Fig. 2.2H, M**). In the five-layered HSMM sheet, HUVECs elongated and connected with each other to form primitive net-shaped aggregates at t = 48 h that further developed at t = 96 h (**Fig. 2.2I, N**). In the seven-layered HSMM sheet, HUVECs also elongated at t = 48 h but were poorly connected and remained sparse net-shaped aggregates at t = 96 h (**Fig. 2.2J, O**).

Table 2.1 Definition of experimental conditions and initial thicknesses of HSMM sheets used in the experiments

Conditions	Layer number of HSMM sheets	Initial thickness of HSMM sheets, *h* (μm)
Control	0	-
Monolayer sheet	1	16.0 ± 3.5
Three-layered sheet	3	26.7 ± 2.2
Five-layered sheet	5	39.1 ± 2.7
Seven-layered sheet	7	55.7 ± 2.9

Thickness values are mean ± SD (n = 3).

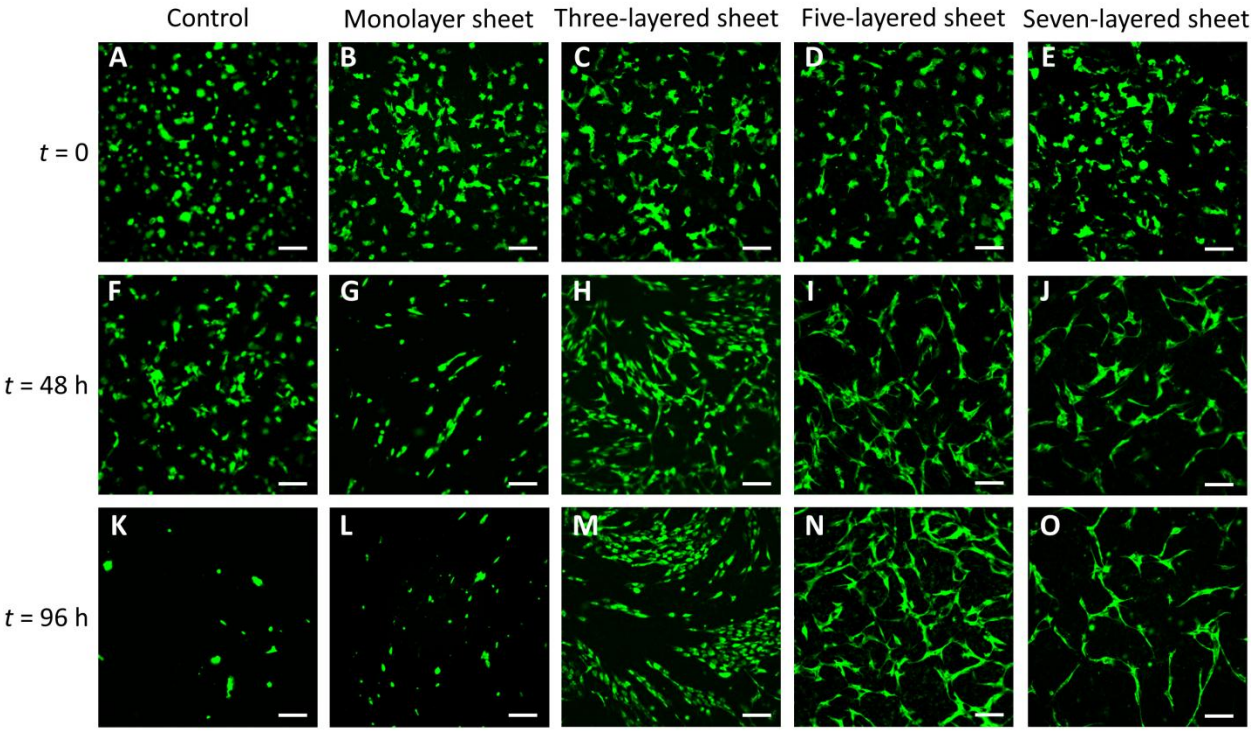

Fig. 2.2 Representative images showing different morphologies of GFP-HUVECs (green) with different layer numbers of HSMM sheets at an incubation time of 0 (A-E), 48 (F-J), and 96 h (K-O).

The morphology of HUVECs that were outside of the cell sheet was also observed at t = 96 h (**Fig. 2.3A-D**). The shape of most HUVECs that were outside of the cell sheet was polygonal and very different from the HUVEC morphologies in the multilayered HSMM sheets. Interestingly, the number of attached HUVECs on the culture surface significantly increased along with the increase in the layer number of the cell sheet (**Fig. 2.3E**). In addition, the numbers of attached HUVECs on the culture surface at 96 h in conditions of the monolayer and three-layered HSMM sheets were 3.9 and 1.7 times lower, respectively, compared to the mean of HUVEC number at the onset of incubation, t = 0, suggesting the HUVEC detachment from the culture surface in these two conditions. However, in conditions of five- and seven-layered HSMM sheets, the numbers of attached HUVECs on the culture surface at 96 h were 1.2 and 2.3 times higher, respectively, compared to the mean of HUVEC number at t = 0, suggesting the HUVEC proliferation on the culture surface in these two conditions.

2.3.2 Localization of HUVECs

To understand the localization of endothelial cells in the vertical direction of the HSMM sheet, GFP-HUVECs were initially put under the cell sheet and their localization at t = 96 h was observed using a confocal laser scanning microscope. It was observed that at t = 96 h, in the monolayer HSMM sheet, HUVECs localized at the top of the cell sheet as single cells (**Fig. 2.4A, E**). The island-shaped aggregates of HUVECs in the three-layered HSMM sheet also localized at the top of the cell sheet (**Fig. 2.4B, F**), whereas the net-shaped aggregates in the five-layered HSMM sheet existed exclusively in the middle of the cell sheet (**Fig. 2.4C, G**). The sparse net-shaped aggregates in seven-layered HSMM sheet localized in the basal layer of the cell sheet (**Fig. 2.4D, H**).

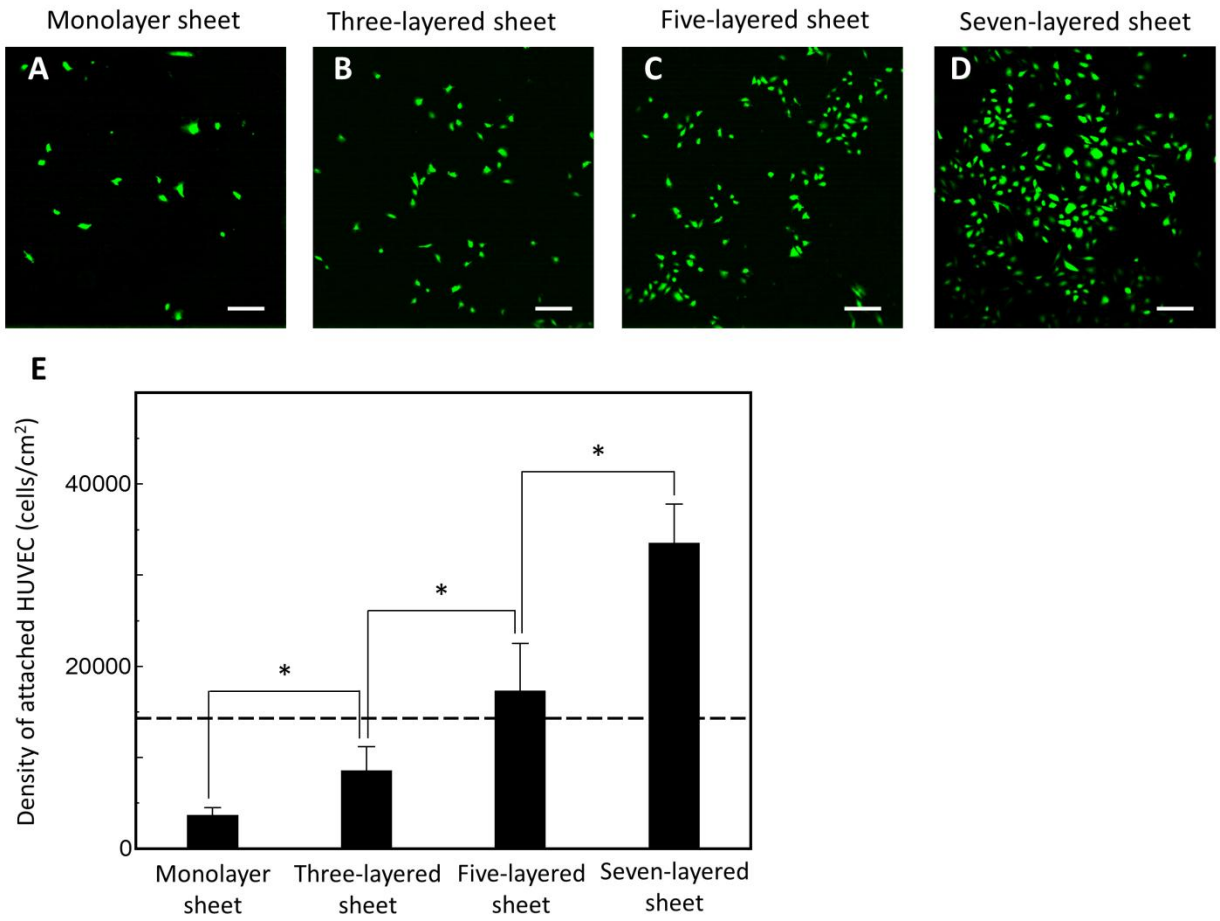

Fig. 2.3 GFP-HUVECs (green) attached on the culture surfaces outside the monolayer (A), three-layered (B), five-layered (C), and seven-layered (D) HSMM sheets at 96 h. Scale bar: 200 μm. Quantitative analysis of HUVEC density outside of the cell sheets (E). The bars show the SD (n = 3). The asterisk shows significant difference ($p < 0.05$). Dash line shows the mean of HUVEC number at the onset of incubation, t = 0.

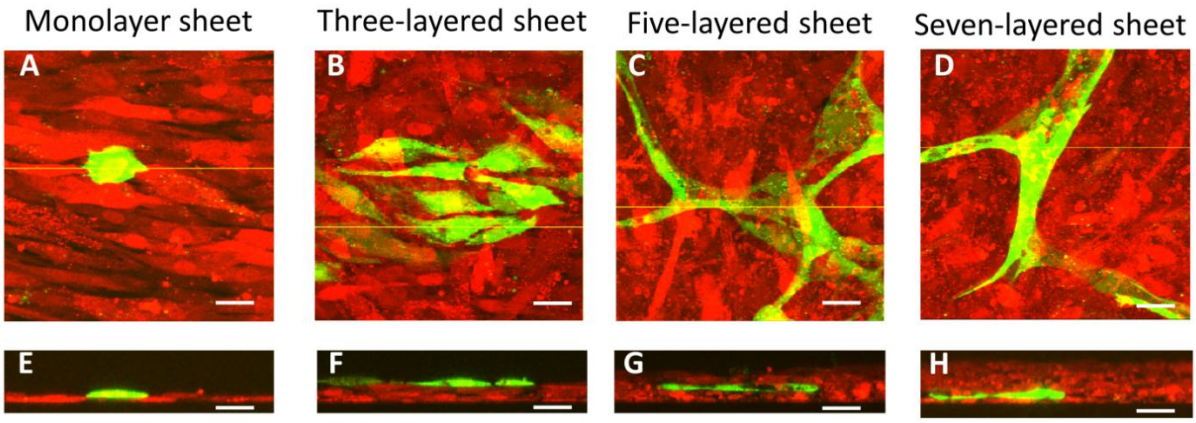

Fig. 2.4 Representative images showing different morphologies and vertical localizations of GFP-HUVECs (green) induced by HSMM sheets (orange) with different layer numbers at 96 h. The *X*-*Y* stacked images (A-D) were constructed from the *X*-*Y* images at 0.6-μm intervals. The *X*-*Z* images (E-H) were constructed along with the yellow lines drawn in the *X*-*Y* stacked images (A-D). Scale bar: 30 μm.

2.3.3 Time-lapse observation of HUVEC behavior inside the HSMM sheet

For further elucidation of endothelial cell behaviors and localization, time-lapse observation was performed (**Fig. 2.5**). In the monolayer HSMM sheet, HUVECs quickly migrated from the bottom upward the top of the cell sheet and detached from t = 14 h. The detachment of HUVECs at the top of the monolayer sheet was continuously observed during the latter incubation, and finally resulted in few remaining cells in the cell sheet. In the three-layered HSMM sheet, HUVECs actively migrated and reached the top layer within t = 46 h. The HUVECs maintained adhesion and formed island-shaped aggregates at the top of the three-layered cell sheet from t = 72 h. In the five-layered HSMM sheet, HUVECs also actively migrated upward with elongated bodies and filopodia within t = 24 h. Migrating HUVECs encountered each other to form net-shaped aggregates before reaching the top of the cell sheet,

and mainly localized in the middle of the five-layered cell sheet from t = 60 h. In the seven-layered HSMM sheet, during 92 h of incubation, HUVECs migrated horizontally near the bottom layer of the cell sheet and formed sparse net-shaped aggregates there.

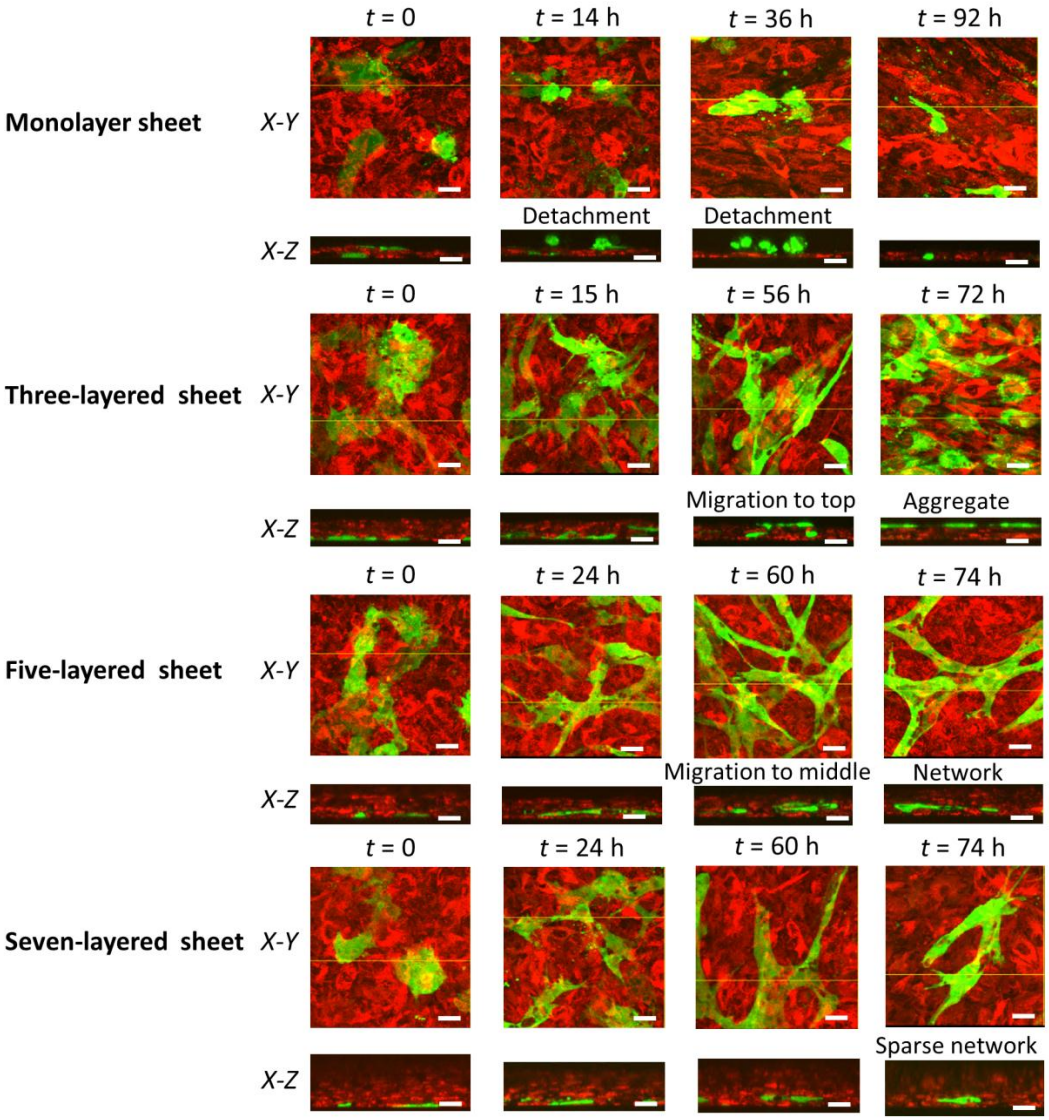

Fig. 2.5 Representative images of time-lapse observation of GFP-HUVECs (green) inside HSMM sheets (orange) with different layer numbers for 92 h of incubation. The *X*-*Y* stacked images were constructed from the *X*-*Y* images at 0.6-μm intervals. The *X*-*Z* images were constructed along with the yellow lines drawn in the *X*-*Y* stacked images. Scale bar: 30 μm.

2.4 Discussion

In the present study, incubation of GPF-HUVECs under HSMM sheets was carried out to understand endothelial cell behavior in the cell sheets. The HUVECs, which initially localized at the bottom of the HSMM sheet, vertically migrated inside the cell sheet. It was revealed that the behaviors and localization of the HUVECs strongly depended on the thickness of the HSMM sheet, which varied along with the layer number of the cell sheet. The thickness of the HSMM sheet might prolong the migration period of the HUVECs from the bottom to the top of the cell sheet to enhance the frequency of HUVEC encounters inside the cell sheet. Herein, the difference of the endothelial morphologies, e.g., the island-shaped aggregate on the top of the cell sheet as a two-dimensional (2D) environment and the net-shaped aggregate inside the cell sheet as a 3D environment, was consistent with findings reported in previous studies. Martin *et al.* described that on 2D substrata with less physical barriers, the endothelial cells formed wide and flat lamellae, whereas in 3D matrices, endothelial cells formed cylindrical branching filopodia (Martins *et al.*, 2006), which play important roles in the exploration of the extracellular matrix and the surface of other cells as well as in the identification of appropriate targets for adhesion (Wood *et al.*, 2002). It is possible that after encountering each other in the 3D cell sheet by using filopodia, endothelial cells form early endothelial cell-cell contacts via VE-cadherin located along filopodia (Almagro *et al*., 2010), making net-shaped aggregates.

On the top of the cell sheet, unconnected HUVECs tended to detach from the monolayer HSMM sheets, whereas HUVECs could remain attached and form island-shaped aggregates on the top of the three-layered HSMM sheets (**Fig. 2.5**). In addition, it was also observed that the attachment of HUVECs on the culture surface outside the HSMM sheet increased with the increase in the layer number of the HSMM sheets (**Fig. 2.3**). These results suggest that the

increment of local HSMM number facilitated the amounts of cytokines, such as VEGF, HGF, and SDF-1, secreted from the HSMMs in the cell sheets (Sekiya *et al*., 2009), which initiated angiogenesis. In the three-layered HSMM sheet, in spite of the HUVEC detachment outside of the cell sheet, it is most likely that the increased quantities of secreted cytokines from the cell sheet improved the attachment among HUVECs, leading to the formation of island-shaped aggregates on the top of the cell sheet. In contrast, the detachment of HUVECs in the control condition and the monolayer HSMM sheet occurred in DMEM containing 10% (v/v) FBS without the addition of any cytokines.

In other studies, endothelial network could be formed in a three-layered cell sheet *in vitro* that was constructed from a mixture of HDFs and HUVECs (Sekiya *et al*., 2010). It was also showed that an endothelial network could be formed in the three-layered sheet of HDF layers and HUVEC layer with a thickness of approximately 20 μm (Asakawa *et al*., 2010). Chapter 1 reported that a high population of HDFs resulted in the decline of overall sheet fluidity (Kino-oka *et al*., 2012). According to this report, the low sheet fluidity of the HDF sheet might reduce HUVEC migration inside the sheet, which allows HUVECs to remain in the sheet longer, and is attributed to the high frequency of network formation. In the present study, the migration of HUVECs and myoblasts can play an important role in affecting the frequency of encounters among HUVECs.

In the present study, a novel 3D *in vitro* culture system, in which GFP-HUVECs and HSMM sheets were co-incubated, was developed using a cell sheet stacking. The thickness of the HSMM sheet, which can be controlled by the layer number of the cell sheet, affected endothelial cell behaviors such as vertical migration, detachment, and formation of the island-shaped and net-shaped aggregates on the top and middle of the cell sheet, respectively.

2.5 Summary

Using a cell sheet stacking method, a 3D *in vitro* culture system was developed by incubating GFP-HUVECs (target cells) under the fluidic scaffold of HSMM sheets (packed cells) with different number of layers, to mimic the *in vivo* angiogenesis in the HSMM sheet after transplantation. The aim in developing this system was to examine the different endothelial behaviors in the cell sheet. During 96 h of incubation, in the monolayer HSMM sheet, HUVECs quickly reached the top of the cell sheet and detached. In the three-layered HSMM sheet, HUVECs also migrated to the top layer and formed island-shaped aggregates. In the five-layered HSMM sheet, HUVECs migrated into the middle of the cell sheet and formed net-shaped aggregates. In the seven-layered HSMM sheet, HUVECs migrated in the basal of the cell sheet and formed sparse net-shaped aggregates. The thickness of the HSMM sheet, which can be controlled by the number of layers in the cell sheet, is therefore an important factor, that affects the migration time, encounters, localization, and morphology of HUVECs inside the HSMM sheet.

Chapter 3

Endothelial network formation process at different seeding densities inside a multilayered myoblast sheet

3.1 Introduction

Autologous transplantation of myoblast sheets has attracted attention as a new technique for curing myocardial infarction, which is associated with cardiomyocyte dysfunction and irreversible cell loss (Memon *et al*., 2005; Miyagawa *et al*., 2011). Skeletal myoblasts have the ability to secrete cytokines which improve heart function via the facilitation of angiogenesis, the process of new capillary formation from pre-existing vessels, and the attraction of progenitors on the affected part. However, the mechanism by which endothelial cells of the host migrate into the transplanted myoblast sheets during angiogenesis remains unclear.

Angiogenesis has been attracting a lot of interest, as it plays a very important role in the development of the embryo, in the reproductive function, wound healing in adults, as well as in many diseases, particularly cancer (Carmeliet, 2005; Folkman, 1995; Munoz-Chapuli *et al.*, 2004; Simons, 2005). Successful control of this process is the key to curing many types of diseases such as cancer, ocular diseases, obesity, diabetes, cardiovascular disease, etc., and overcoming one of the most difficult obstacles in tissue engineering to fabricate thick and viable engineered tissue for transplantation (Cao, 2010; Folkman, 2007).

From a manufacturing point of view, process and quality controls are important for realizing commercialization of cell sheet transplant. Many studies have addressed cell sources, culture, sheet assembling, and *in vivo* animal tests; however, a method for the quality control of myoblast sheets, especially for transplant efficacy such as angiogenesis capability, has not been

systematized yet. To understand the angiogenesis process, many models have been proposed (Auerbach *et al.*, 2003). Of course, the *in vivo* tests are very important to observe the overall effects of experiments on the living subjects, but normally require special training, and are quite expensive and time consuming (Auerbach *et al.*, 2003). Some conventional *in vitro* testing models, both in 2D and 3D, such as Matrigel, collagen and biodegradable materials, have also been used, in spite of some of their limitations (Asakawa *et al.*, 2010; Auerbach *et al.*, 2003; Black *et al.*, 1998; Manoussaki *et al.*, 1996; Serini *et al.*, 2003; Tsigkou *et al.*, 2010; Unger *et al.*, 2007; van der Meer *et al.*, 2010; Vernon *et al.*, 1999). For example, Matrigel was used to study the network formation of endothelial cells. However, some other non-endothelial cells such as fibroblast, or tumor cells, also presented a network-like formation on Matrigel. To approach the full understand of angiogenesis, the use of 3D tissue models with quantitative analysis is strongly needed.

In previous chapters, by utilizing the advantages of cell sheet technology, the author constructed a novel 3D *in vitro* culture system, which is an imitation of the transplanted cell sheet and the host, in order to understand the endothelial behavior inside HSMM sheets. The five-layered myoblast sheet was revealed to be the optimal 3D structure for endothelial cells to form a network. In this chapter, image processing was performed to quantitatively evaluate the HUVEC spatial distribution and network formation in the HSMM sheet, so as to elucidate the spatial habitation arising from HUVEC migration and connection.

3.2 Materials and methods

3.2.1 Cell culture

HSMMs (Lot. No. 4F1618; Lonza Walkersville Inc., Walkersville, MD, USA) and HUVECs (Lot.No.4F0709; Lonza Walkersville Inc.) were used in the experiments. According to procedures described elsewhere (Chowdhury *et al*., 2010), subcultures of HSMMs on laminin-coated surfaces were conducted at 37 °C in an atmosphere of 5% CO_2 in Dulbecco's Modified Eagle's Medium (DMEM; Sigma-Aldrich, St. Louis, MO, USA) containing 10% (v/v) fetal bovine serum (FBS; Invitrogen, Grand Island, NY, USA) and antibiotics (100 U/cm^3 penicillin G, 0.1 mg/cm^3 streptomycin, and 0.25 mg/cm^3 amphotericin B; Invitrogen). HUVECs were cultured in a commercially available medium (EGM-2; Lonza Walkersville Inc.). The medium depth was set to 2 mm throughout the experiments.

3.2.2 Incubation of five-layered HSMM sheet with HUVECs

Five-layered HSMM sheet (packed cells) was fabricated according to a previously reported method in Chapter 2. In brief, starter HSMMs were stained with CellTracker™ Orange (Invitrogen) and seeded at 2.3×10^5 cells/cm^2 into each well of 24-well UpCell™ plates (CellSeed, Tokyo, Japan) which was mounted in advance with Teflon rings to improve the detachment of the cell sheet in the harvesting operation. The final culture area in each well was 0.95 cm^2. Cells seeded in UpCell™ plates which have temperature-responsive surfaces grafted with PIPAAm were incubated for 24 h at 37 °C in a 5% CO_2 atmosphere to form the monolayer sheet. To stack monolayer sheets to fabricate the multilayered cell sheet, the customized stamps with the gelatin gel (G1890-100G; Sigma-Aldrich) were used. To harvest the monolayer sheet, the stamp with the

gelatin gel was overlaid on the monolayer sheet in a well at 37 °C, and the temperature was shifted to 20 °C. After 30 min, the stamp was lifted together with the monolayer sheet from the bottom surface of the well. The steps were then repeated for the sequential harvests of monolayer sheets to form the multilayered construct on the stamp. The multilayered sheet with the gelatin was peeled from the stamp for transfer to a dish containing the precultured HUVECs (target cells). For the preculture, HUVECs were seeded into culture dishes (35 mm in diameter; Corning Inc., NY, USA) and cultured in the EGM-2 medium supplemented with 20% (v/v) FBS for 24 h. The initial density of HUVECs (X_0) for the subsequent incubation with the sheet was set in the range of 0.35 to 3.32 × 10^4 cells/cm^2 by changing the seeding density of HUVECs (X_S). The relationship between X_S and X_0 was determined in advance (**Table 3.1**). After incubation at 20 °C for 2 h, the sheet was incubated at 37 °C in DMEM containing 10% FBS for 1 h to remove the gelatin. The medium containing the dissolved gelatin was exchanged with fresh medium. At the given incubation time (t), triplicate samplings were performed for quantitative analysis. During the incubation period, the medium was renewed every day.

Table 3.1 Relationship between seeding densities (X_S) and initial densities (X_0) of HUVEC

Seeding density, X_S (10^4 cells/cm^2)	Initial density, X_0 (10^4 cells/cm^2)
0.2	0.35 ± 0.04
0.5	0.69 ± 0.11
1.0	1.29 ± 0.23
1.5	2.20 ± 0.16
2.0	3.32 ± 0.16

X_0 values are mean ± SD (n = 3).

3.2.3 Immunostaining for HUVECs

The culture system containing the five-layered HSMM sheet with HUVECs was washed with phosphate-buffered saline (PBS) and fixed in PBS containing 4% (v/v) paraformaldehyde (Wako Pure Chemical Industries, Osaka, Japan) overnight. The fixed specimen was then permeabilized in PBS containing 0.1% (v/v) Triton X-100 (Wako Pure Chemical Industries) for 12 min, washed twice with PBS, and then blocked in 1% (v/v) bovine serum albumin (BSA; Wako Pure Chemical Industries) in PBS for 1 h. The specimen was labeled with a primary antibody (monoclonal mouse anti-human CD31 antibody; DAKO, Glostrup, Denmark) in 1% (v/v) BSA solution overnight. The specimen was then thoroughly washed with PBS and immersed in 1% (v/v) BSA solution containing the secondary antibody conjugated with Alexa Fluor® 488 (Invitrogen) for 1 h.

3.2.4 Evaluation of the HUVEC network formed inside the HSMM sheet

The image capture was carried out using a 10× objective lens of confocal laser scanning microscope (FV-300; Olympus, Tokyo, Japan) at more than 8 positions in each sample. As shown in **Fig. 3.1A**, each image was 8-bit gray scale with a size of 256 × 256 pixels and covered an area of 942 × 942 μm. The images were subjected to image processing (Image-Pro Plus; Media Cybernetics Inc., Bethesda, MD, USA) using a low-pass filter for primary noise removal and binarization with a certain intensity threshold. The threshold intensity was determined as the average of the mode intensity and the automatic threshold intensity calculated with an Otsu adaptive threshold algorithm (Otsu, 1979), which chooses the threshold to minimize the intra-class variance of the thresholded black and white pixels with an exhaustive search. The binary images were subjected to skeletonization to produce lined objects and dilation, the secondary

noise removal with a size threshold to remove items with a size of less than 16 pixels, and the pruning of small branches in the objects. The total length of the network per image area (L; cm^{-1}), and the number of total tips of the network (N_T; tip/cm^2), were measured to estimate the extent of the HUVEC network (L/N_T; cm/tip). The tips existing at the edge of the image were not counted.

3.2.5 Spatial distribution of HUVECs and HSMMs in five-layered HSMM sheets

To determine the vertical distribution of the HUVECs inside the HSMM sheet, the green cells (HUVECs labeled with Alexa Fluor® 488) and orange cells (HSMMs stained with CellTracker™ Orange) in each layer were observed and quantitatively analyzed as previously described in Chapter 1 (Kino-oka *et al.*, 2012) (**Fig. 3.1B**). The number of colored pixels in each slice was counted. The orange pixels in each slice were normalized using the maximum orange pixel values, found in all of the slice images. Slices possessing more than 10% of the orange pixels were regarded to exist inside the cell sheet, from which the vertical positions at the top and bottom of the five-layered sheet, and the sheet thickness, h, were determined. The green pixels inside the sheet were normalized to determine the vertical distribution of the green pixels by dividing them into 5 layers. The normalized distribution of the green pixels was assumed to be equivalent to the distribution of green cells in the sheet, which was determined as the frequency of green cells, f_G (-), in each layer. For determination of the vertical distribution of the HSMMs, HSMMs stained with CellTracker™ Green (Invitrogen) were placed in the bottom layer of a five-layered HSMM sheet, and their vertical distribution at 24 h was determined.

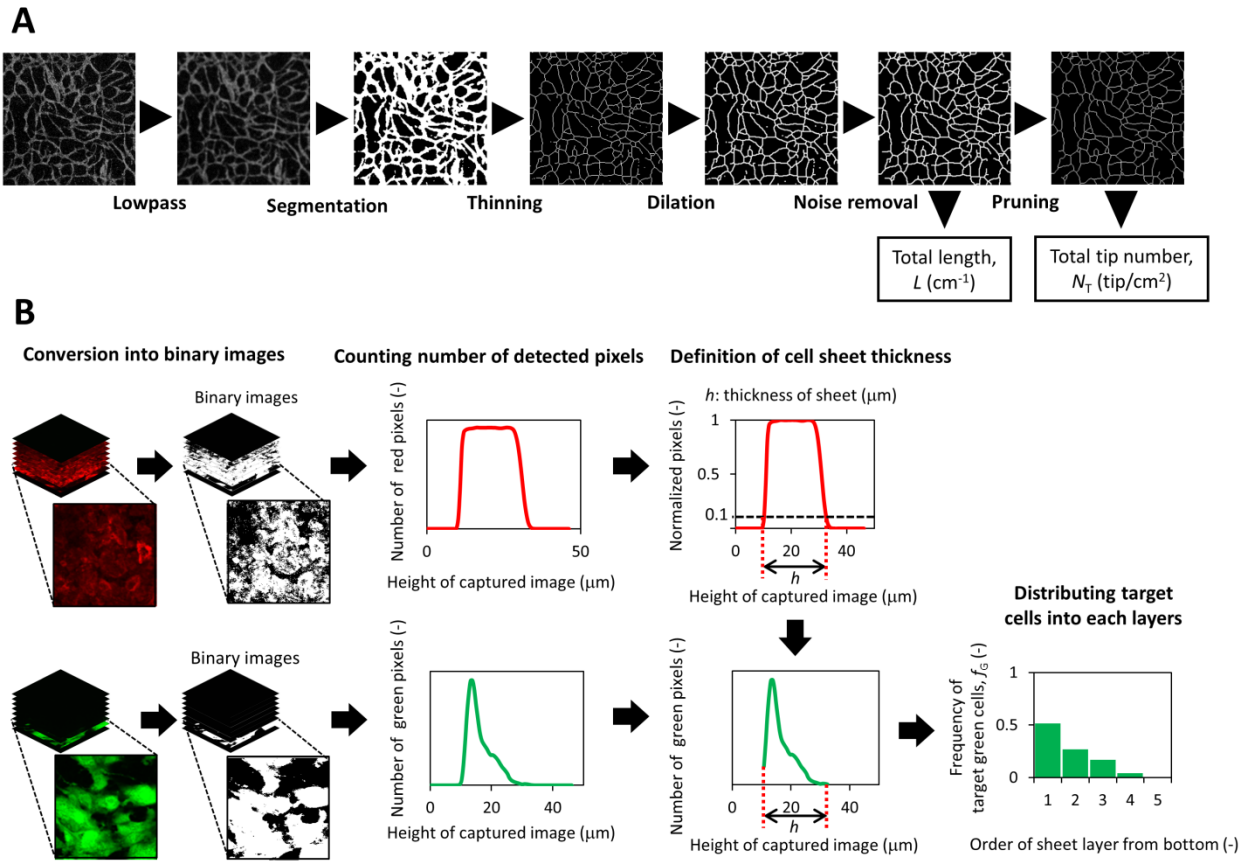

Fig. 3.1 Image process procedure to evaluate HUVEC network formation and maturation (A) and HUVEC localization in 3D myoblast sheet (B).

3.3 Results

3.3.1 HUVEC network formation inside the HSMM sheet

The behavior of HUVECs in the five-layered HSMM sheet was observed for 120 h to estimate the growth and network formation according to the parameters L, N_T, and L/N_T. The initial density of HUVECs was set at $X_0 = 1.29 \times 10^4$ cells/cm^2. At the beginning of the incubation period ($t = 0$), as shown in **Fig. 3.2**, the HUVECs were observed to be single and round-shaped with podia. At $t = 24$ h, most of the HUVECs were found to have elongated for initiation of migration in the sheet, resulting in an increase in L. With further prolongation of the incubation period beyond $t = 48$ h, the level of L was constant, i.e., the HUVECs did not grow further. In addition, the HUVECs began to encounter and connect with each other, resulting in a decrease in N_T until $t = 96$ h. Smooth connections of the HUVECs appeared at $t = 96$ h, which suggested the maturation of the HUVEC network. These behaviors were reflected by an increase in L/N_T although a slight decay of the connections occurred at $t = 120$ h. The maximum value of L/N_T was = 0.22 ± 0.07 cm/tip at $t = 96$ h, which was 5.6 times higher than the value at $t = 24$ h.

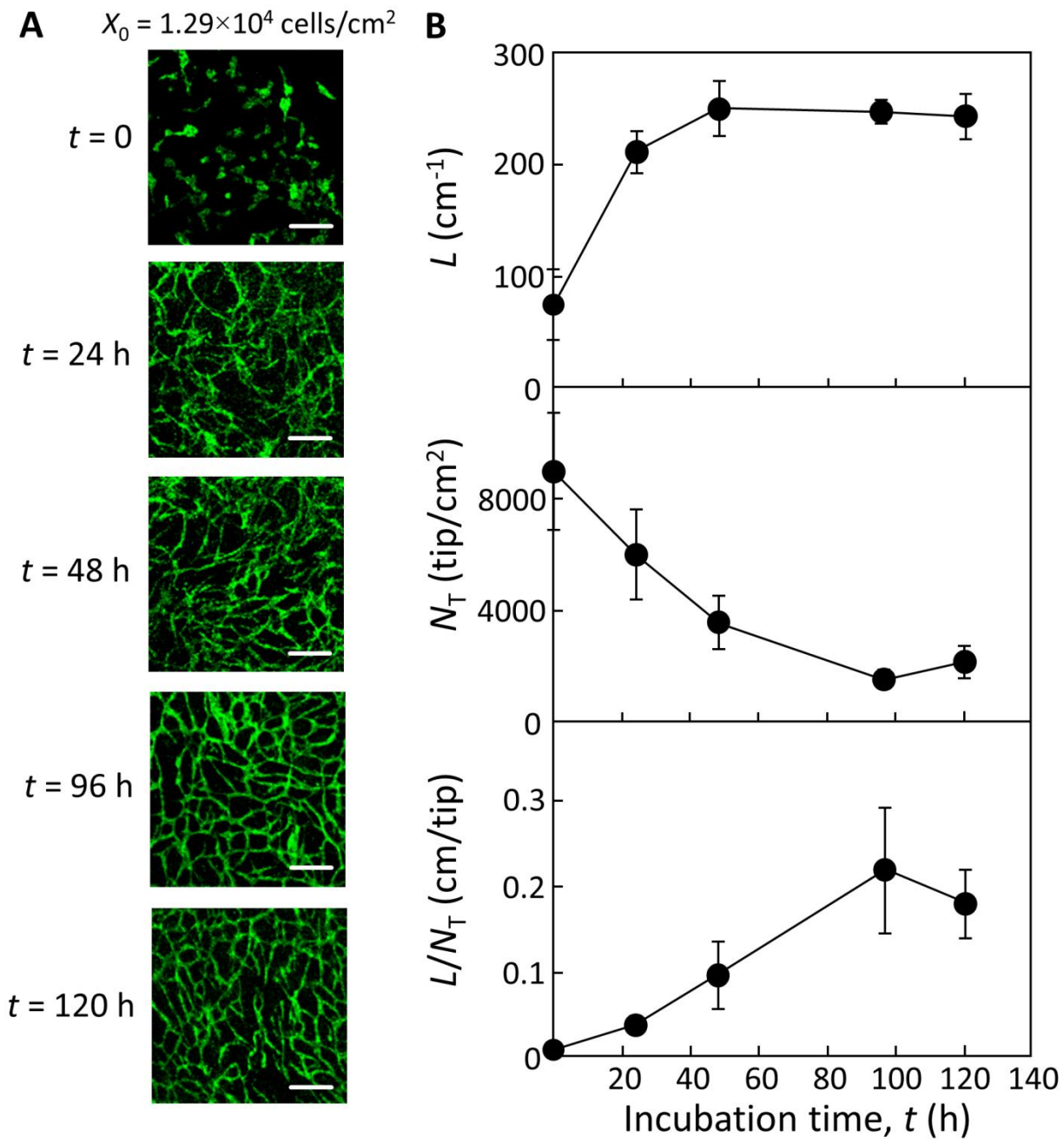

Fig. 3.2 Time course of HUVEC network formation inside the five-layered HSMM sheet at an initial HUVEC density (X_0) of 1.29 × 10^4 cells/cm^2. (A**)** Horizontal images of HUVEC morphology. Scale bar: 200 μm. (B**)** Evaluation of HUVEC network formation with image processing. L: total length (cm^{-1}), N_T: total tip number (tip/cm^2), L/N_T: extent of network formation (cm/tip). The bars show the SD (n = 3).

3.3.2 Vertical migration of HUVECs during network formation

During network formation, the HUVECs were initially localized at the bottom of the HSMM sheet and then vertically migrated into the inner portion of the sheet to form aggregates with a lumen structure inside the sheet (**Fig. 3.3**). To estimate the vertical migration of the HUVECs, their spatial distribution pattern was obtained as shown in **Fig. 3.4**. At the beginning (t = 0), the frequency of green cells (HUVECs) f_G was the highest in the first layer from the bottom surface, i.e., most of HUVECs were located at the bottom of the HSMM sheet. A broader distribution of f_G was obtained at t = 24 h, meaning the HUVEC migration toward the upper layers of sheet. In addition, the migration of the HUVECs was much faster than that of HSMMs because of the broader distribution of the HUVECs at t = 24 h (**Fig. 3.5**). At t = 96 h, HUVECs inhabited the middle layer, with f_G = 0.40 and 0.30 in the second and third layers, respectively, which was higher than the values in the corresponding bottom and top layers. **Fig. 3.4B** depicts the aggregate shape of the HUVECs in the sheet at t = 96 h. The HUVECs in the middle layer formed a net-shaped aggregate to generate the network, whereas those in the top layer formed an island-shaped aggregate, which indicates that the shape of the HUVEC aggregate depended on their location in the sheet.

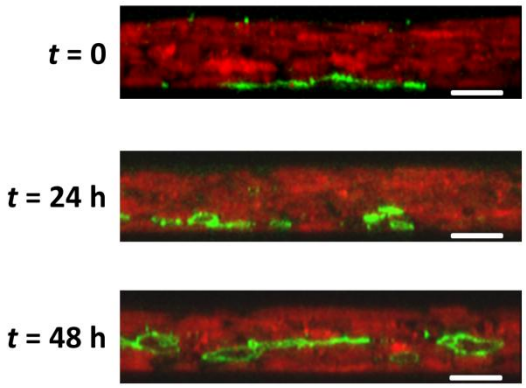

Fig. 3.3 Typical confocal laser scanning microscopy images showing a cross section of an HSSM sheet with HUVECs during network formation with an initial HUVEC density (X_0) of 1.29×10^4 cells/cm^2. Scale bar: 20 μm.

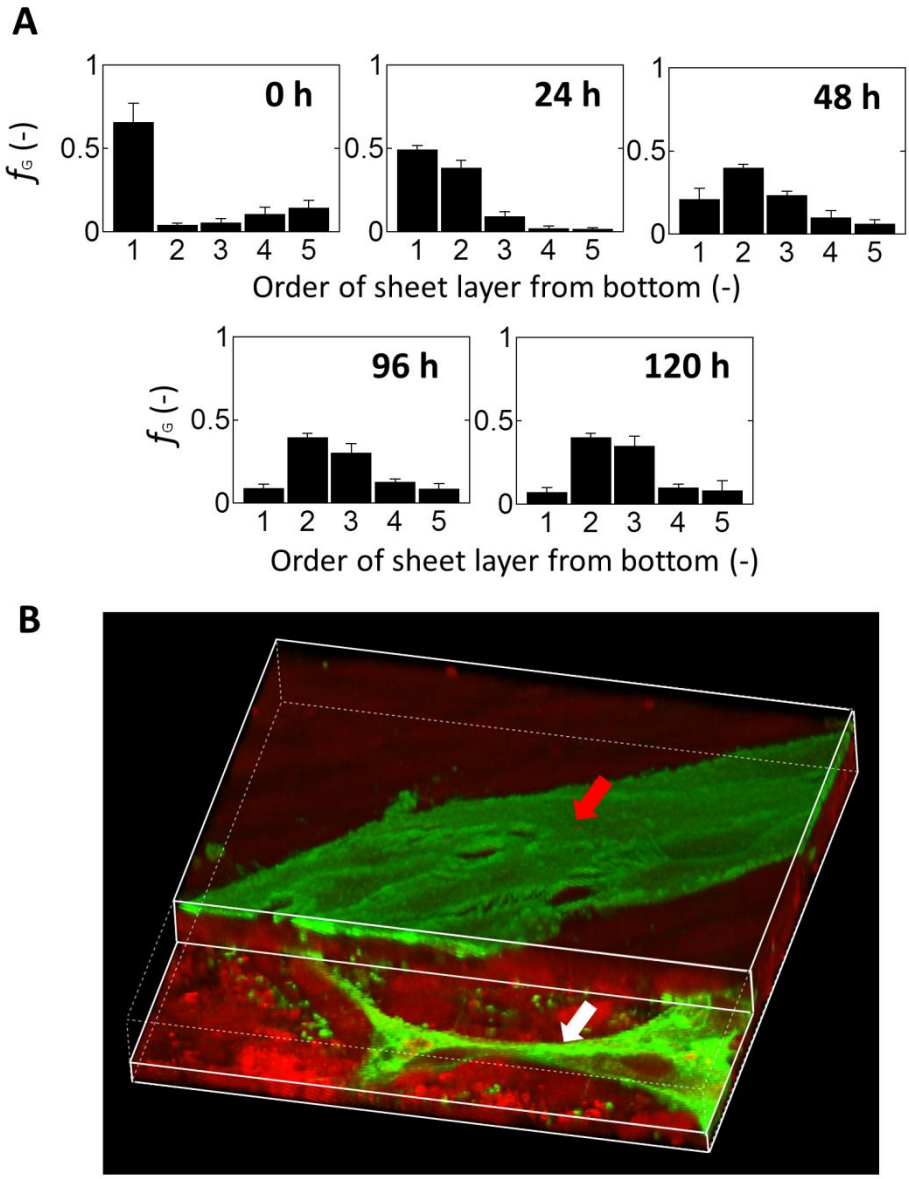

Fig. 3.4 Vertical analysis of HUVEC network formation inside the five-layered HSMM sheet at an initial HUVEC density (X_0) of 1.29 × 10^4 cells/cm^2. (A**)** Time course of the spatial distribution of HUVECs (f_G) in each layer of the HSMM sheet. Bars show the SD (n = 3). (B) Three-dimensional image of HSMM sheet showing different shapes of HUVEC aggregates at different positions in/on the sheet at t = 96 h. The white arrow indicates net-shaped aggregation (network) in the middle layer of the cell sheet. The red arrow indicates island-shaped aggregation in the top layer on the cell sheet.

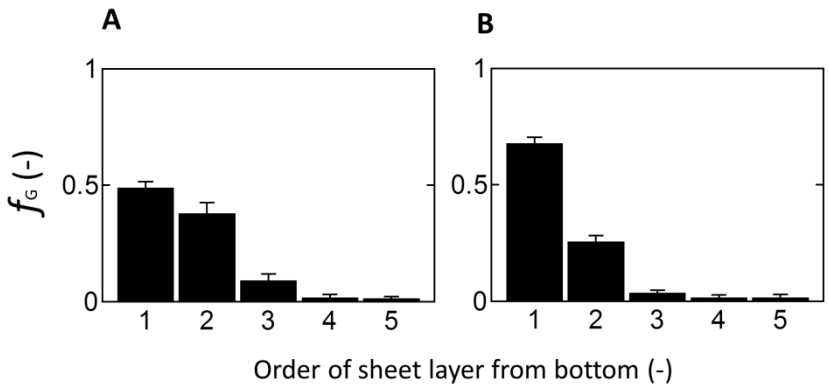

Fig. 3.5 Spatial distribution of the green target cells inside the cell sheet at 24 h. The bars show the SD (n = 3). (A) Frequency of HUVECs (f_G) in each layer of the five-layered HSMM sheet. (B) Frequency of HSMMs in each layer of the five-layered HSMM sheet.

3.3.3 Influence of HUVEC seeding density on migration and network formation

To evaluate the HUVEC connectivity in the sheet, the HUVECs were incubated for t = 96 h with initial densities ranging from $X_0 = 0.35 \times 10^4$ to 3.32×10^4 cells/cm^2. As shown in **Fig. 3.6**, with an increase in X_0, L/N_T increased to a maximum value of L/N_T = 0.484 cm/tip at $X_0 = 2.20 \times 10^4$ cells/cm^2, which was 2.3 times higher than the value at $X_0 = 1.29 \times 10^4$ cells/cm^2. In addition, the length and tip number of the HUVECs were estimated on the basis of the parameters such as specific length (L/X_0) and specific tip number (N_T/X_0), respectively. The L/X_0 and N_T/X_0 decreased with an increase in X_0 by $L/X_0 = 9.0 \times 10^{-3}$ cm/cell and $N_T/X_0 = 5.0 \times 10^{-2}$ tip/cell at $X_0 = 3.32 \times 10^4$ cells/cm^2, which was 3 and 30 times lower than the value at $X_0 = 0.35 \times 10^4$ cells/cm^2, respectively.

The f_G value of HUVECs at 96 h in the first, third, and fifth layers with respect to the initial density is shown in **Fig. 3.7**. In the fifth layer (top layer), with an increase in X_0, f_G decreased to 0.07 at $X_0 = 1.29 \times 10^4$ cells/cm^2, which was half of the value at $X_0 = 0.35 \times 10^4$ and 0.69×10^4

cells/cm^2. A further increase in X_0 resulted in a slight increase of f_G to 0.10 at X_0 = 3.32 × 10^4 cells/cm^2. This trend was contrary to that observed in the third layer (middle layer).

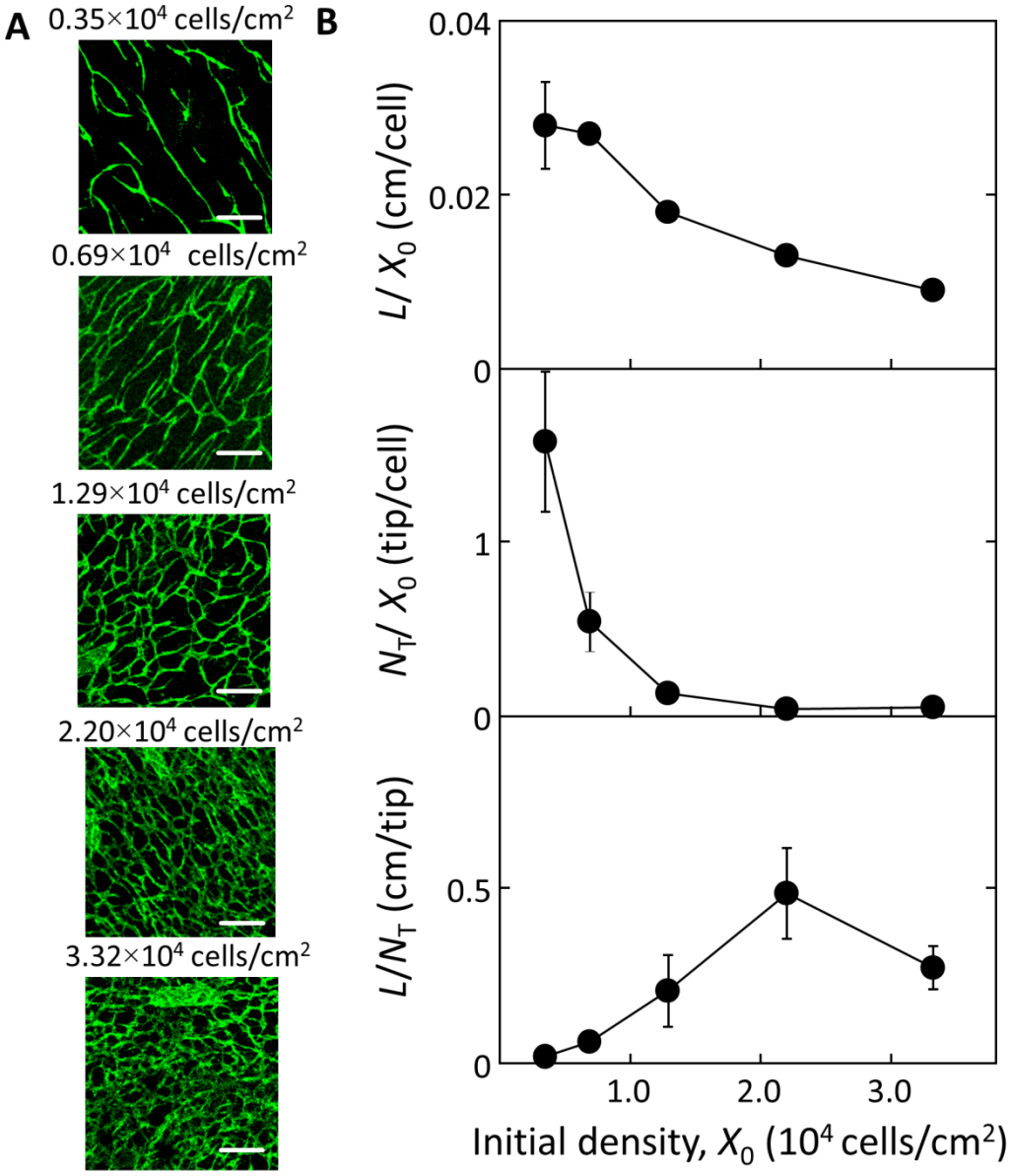

Fig. 3.6 Network formation at 96 h with different initial densities of HUVECs (X_0) ranging from 0.35 × 10^4 to 3.32 × 10^4 cells/cm^2. (A**)** Horizontal images of HUVEC morphology. Scale bar: 200 μm. (B) Evaluation of HUVEC network formation with image processing. L/X_0: specific length (cm/cell), N_T/X_0: specific tip number (tip/cell), L/N_T: extent of network formation (cm/tip). The bars show the SD (n = 3).

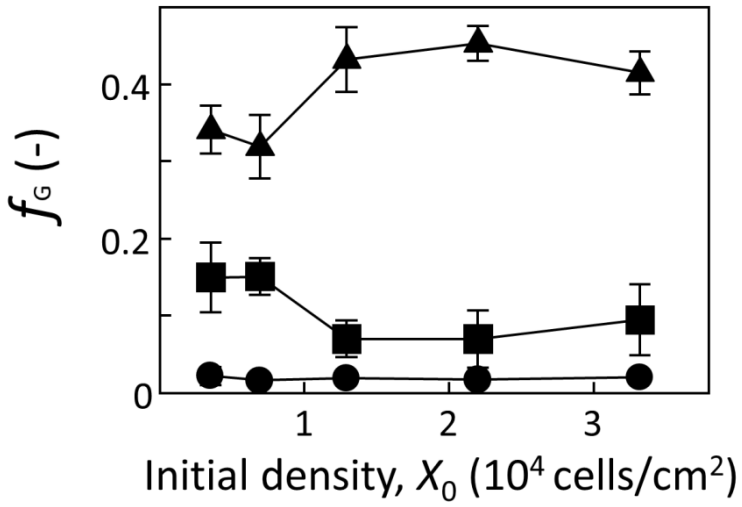

Fig. 3.7 Spatial distribution of HUVECs at 96 h with different initial densities of HUVECs (X_0) ranging from 0.35 × 10^4 to 3.32 × 10^4 cells/cm^2. Frequency of HUVECs (f_G) in the top (square), middle (triangle) and bottom (circle) layers are shown against X_0. Bars show the SD (n = 3).

3.4 Discussion

Cell migration in 3D constructs plays an important role in physiological and pathological phenomena such as embryonic development, cell alignment, immune reactivity, angiogenesis, and metastasis (Horwitz *et al.*, 2003b). Determining the mechanisms underlying cell migration in 3D tissues having fluidity will be useful for designing biomimetic structures and functionally engineered tissues. Although the behaviors of cells on 2D culture surfaces or in static 3D scaffold have been extensively investigated, cell movement in fluidic 3D tissues, especially vertical migration inside the tissue, has not been well addressed because of the absence of *in vitro* methods which enable quantitative and reproducible measurements. In the present study, a five-layered HSMM sheet was fabricated as a 3D *in vitro* culture system to evaluate vertical cell migration by confocal laser scanning microscopy with image processing. The author also

established the mimic system of transplantation consisting of HUVECs on a culture dish that represent target cells at the lesion site as well as a five-layered HSMM sheet as the transplant tissue. This system can be used to model angiogenesis after transplantation. The HUVECs that were initially localized at the bottom of the HSMM sheet vertically migrated into the inner portion of the sheet. The migrating HUVECs encountered and connected with other HUVECs in the middle layer of the sheet to form a network (**Figs. 3.2 and 3.4**). In Chapter 1, the active fluidity by the migrations of HSMMs in the horizontal and vertical directions in the five-layered HSMM sheet was observed. The results of the present study revealed that the vertical migration of HUVECs was higher than that of HSMMs (**Fig. 3.5**), demonstrating the active migration of HUVECs in a fluidic sheet.

The formation of HUVEC network regarded as a net-shaped aggregate was localized in the middle layer of the sheet owing to the encountering of HUVECs and their linear connections, while the unconnected HUVECs continued to migrate toward the top layer, forming the island-shaped aggregate (**Fig. 3.4**). These results show that the spatial habitation of HUVECs occurred in the top and middle layers of the sheet by their encountering and connection. In addition, the shape of the HUVEC aggregates depended on their location in the sheet. The further performance of HUVEC behavior at different densities supported the habitation (**Figs. 3.6 and 3.7**), revealing that the HUVECs were localized both in the middle and the top layer at the low initial densities (X_0 = 0.35 × 10^4 and 0.69 × 10^4 cells/cm^2), while only in the middle layer at the higher initial densities (X_0 = 1.29 × 10^4 and 2.20 × 10^4 cells/cm^2). These results led to the mechanism for the spatial inhabitation as follows. As shown in **Fig. 3.8**, the frequency of encountering of HUVECs at a low concentration caused less connectivity in the middle layer of the sheet, and unconnected free HUVECs continued to migrate upward. With an increase in the

HUVEC density in the sheet, the HUVECs exhibited a higher frequency of encountering to connect each other (at a moderate concentration). Excessive existence of HUVECs leads to less sites for their connection although higher frequency of encountering occurred, resulting in the larger number of HUVECs migrating toward top layer.

The dependence of the shape of the HUVEC aggregate on the location of the cells in the sheet was reported in previous studies. Asakawa *et al*. reported that HUVECs in multilayered sheet of human dermal fibroblasts formed a network with a tubular structure when the HUVECs were initially set in the middle layer of the sheet (Asakawa *et al*., 2010). On the other hand, the introduction of HUVECs in the top layer of the sheet generated the island-shaped aggregates; thus the HUVEC habitation in the top and middle layers depended on the initial location of the HUVECs in the sheet. In the present study, the HUVECs outside the sheet did not grow in DMEM including 10% FBS due to no additional cytokines (data not shown). Thus, the network formation in the sheet could be attributed to the local feeding of cytokines from HSMMs. Candidate cytokines secreted from HSMMs are considered to be vascular endothelial growth factor (VEGF), hepatocyte growth factor (HGF) and basic fibroblast growth factor (bFGF) (Hawke and Garry, 2001) which affect endothelial cell division, migration, and connection mediated by VE-cadherin expression (Esser *et al*., 1998; Lamalice *et al*., 2007; Underwood *et al*., 2002).

The fabrication of aggregates, which is a minimum unit exhibiting tissue function, has been required to propose angiogenesis models (Levenberg *et al*., 2005). A sphere-shaped aggregate is widely used as a platform for 3D models or bio-mimic assay. However, histological analysis is necessary to evaluate the HUVEC network in the sphere-shaped aggregate, leading to a difficulty in observation (Kunz-Schughart *et al*., 2006; Rouwkema *et al*., 2006; Timmins *et al*., 2004). In

this study, the system with a widespread HUVEC network in a multilayered sheet regarded as a plate-shaped aggregate enables the independent observation of the vertical and horizontal distributions of cells in 3D constructs via one-dimensional (*Z*-axis) and two-dimensional (*XY*-axis) analyses, being a powerful tool for *in vitro* angiogenesis assays, which can evaluate the HUVEC behaviors such as migration, connection, as well as the formation of an endothelial network in a 3D construct.

In conclusion, a five-layered HSMM sheet (packed cells) and HUVECs (target cells) which mimic the *in vivo* transplantation system was developed. The HUVECs that were initially localized at the bottom of the HSMM sheet, exhibited vertical migration into the inner portions of the sheet, and formed networks in the middle layer of the sheet. The quantitative analysis of the vertical distribution of HUVECs in the sheet clarified the process of their network formation. Spatial habitation of the HUVEC network in the middle layer of the sheet was observed and the extent of the network formation depended on the frequency of encountering between HUVECs. The system in this study including widespread formation of HUVEC network in a fluidic scaffold and its evaluation method might be applicable not only for the *in vitro* construction of pre-vascularized tissue but also for *in vitro* angiogenesis models.

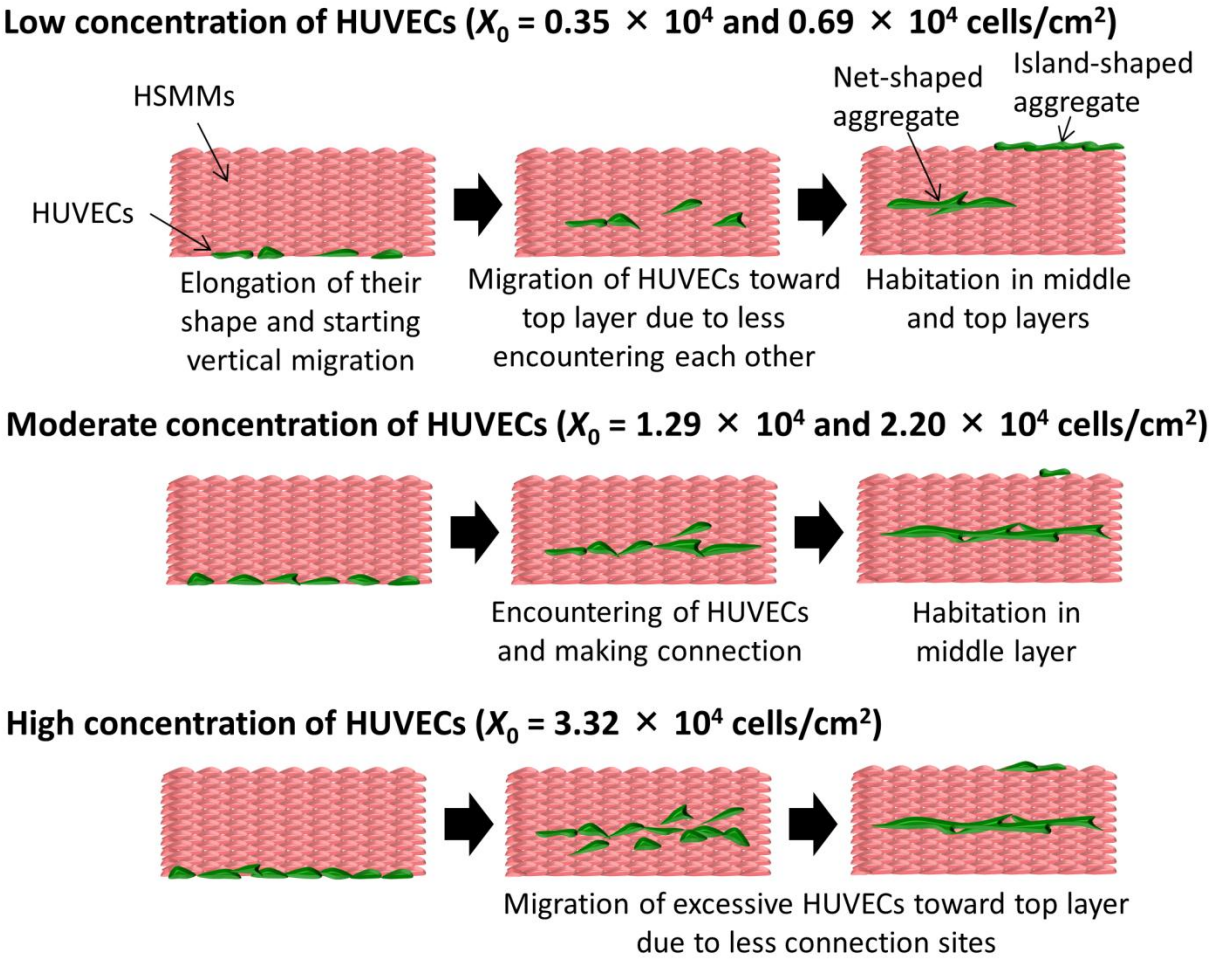

Fig. 3.8 Schematic illustration showing the probable behaviors of HUVECs in the HSMM sheet with various HUVEC initial densities.

3.5 Summary

Using the 3D *in vitro* culture system, the author investigated the detailed dynamic behaviors of endothelial cells (target cells) during the network formation process inside a multilayered myoblast sheet (packed cells). An image processing method was developed to quantitatively analyze the total length, total tip number and the extension of the network, which show the detailed cell behavior and the quality of the network. HUVECs at the bottom of the HSMM sheet became elongated, actively migrated upward, encountered and connected to form a network in the middle of the HSMM sheet from 0 to 96 h of incubation, and finally degraded at 120 h. Non-networked HUVECs continued to migrate to the top of the sheet, indicating the spatial habitation of HUVECs in the cell sheet. The evaluation of network extension using image processing showed that the initial density of HUVECs strongly affected the quality of the endothelial network formation. The present 3D *in vitro* culture system, which can evaluate the endothelial network formation, is considered to be a promising 3D *in vitro* angiogenesis model.

General Conclusion

In present study, through the establishment of a novel 3D *in vitro* culture system with quantitative analysis, the endothelial behavior during network formation inside a multilayered myoblast sheet was clarified. Several factors, such as thickness of the cell sheet, culture time and density of endothelial cells can be controlled in future designs, in order to improve quality of the engineered cell sheet. The major findings in this research are concluded as follows.

In chapter 1, the procedure for fabricating a multilayered cell sheet was developed by using cell sheet technology. The target cells and packed cells were live-stained with different colors, and seeded at high density onto a temperature-responsive culture surface, to form a monolayer cell sheet after 24 h of incubation. The monolayer cell sheets were detached simply by lowering the temperature of the culture surface to 20 °C, and stacked together to form a multilayered cell sheet using a customized stamp system with gelatin. Confocal laser scanning microscopy revealed the dynamic migration of myoblasts inside cell sheet to be sheet fluidity. Image processing was improved to evaluate the vertical spatial distribution of target cells, indicating the vertical migration of cells during 48 h of incubation, similar to molecular diffusion. Parameter diffusivity was estimated to show the effect of HDF addition on sheet fluidity. This 3D fluidic scaffold was used in the following chapters to construct a 3D *in vitro* culture system used for understanding the endothelial behavior during network formation process.

In chapter 2, a 3D *in vitro* culture system was developed by incubating GFP-HUVECs (target cells) under the fluidic scaffold of HSMM sheets (packed cells) with different number of layers, to mimic the *in vivo* angiogenesis in the HSMM sheet after transplantation. The aim in developing this system was to examine the different endothelial behaviors in the cell sheet. During 96 h of incubation, in the monolayer HSMM sheet, HUVECs quickly reached the top of

the cell sheet and detached. In the three-layered HSMM sheet, HUVECs also migrated to the top layer and formed island-shaped aggregates. In the five-layered HSMM sheet, HUVECs migrated into the middle of the cell sheet and formed net-shaped aggregates. In the seven-layered HSMM sheet, HUVECs migrated in the basal of the cell sheet and formed sparse net-shaped aggregates. The thickness of the HSMM sheet, which can be controlled by the number of layers in the cell sheet, is therefore an important factor, which affects the migration time, encounters, localization, and morphology of HUVECs inside the HSMM sheet.

In chapter 3, using the 3D *in vitro* culture system, the author investigated the detailed dynamic behaviors of endothelial cells (target cells) during the network formation process inside a multilayered myoblast sheet (packed cells). An image processing method was developed to quantitatively analyze the total length, total tip number and the extension of the network, which show the detailed cell behavior and the quality of the network. HUVECs at the bottom of the HSMM sheet became elongated, actively migrated upward, encountered and connected to form a network in the middle of the HSMM sheet from 0 to 96 h of incubation, and finally degraded at 120 h. Non-networked HUVECs continued to migrate to the top of the sheet, indicating the spatial habitation of HUVECs in the cell sheet. The evaluation of network extension using image processing showed that the initial density of HUVECs strongly affected the quality of the endothelial network formation. The present 3D *in vitro* culture system, which can evaluate the endothelial network formation, is considered to be a promising 3D *in vitro* angiogenesis model.

In summary, through the establishment of a novel 3D *in vitro* culture system with quantitative analysis, the endothelial behavior during network formation inside a multilayered myoblast sheet was clarified. Several factors, such as thickness of the cell sheet, culture time and density of endothelial cells can be controlled in future designs, in order to improve quality of the

engineered cell sheet. The findings in this study are applicable to angiogenesis research, drug screening, and the design of multilayered myoblast sheets for curing myocardial infarction.

Overall, this study has successfully established a novel 3D *in vitro* culture system, including fluidic multilayered myoblast sheet (the packed cells as transplanted cell sheet) and endothelial cells (the target cells as host blood vessels), to mimic the *in vivo* angiogenesis. The advantage of this research is that, by using live cell staining and using different observation methods, the cell behaviors inside plate-shaped cell sheet can be easily observed and analyzed independently in 2D horizontal (*X*-*Y*) or 1D vertical (*Z*) direction using improved image processing methods applicable in quality control. The 3D *in vitro* culture system in this research is considered to overcome the complexities and difficulties in the conventional *in vivo* tests or *in vitro* models using 3D sphere-shaped aggregates and 2D hydrogels. The mechanism of endothelial behaviors during network formation, the initial step of angiogenesis, was clarified by taking into consideration various factors, such as the thickness of the cell sheet, the culture time, and the density of the endothelial cells. The broad, well-connected endothelial network obtained in multilayered myoblast sheet as prevascularization is likely to be successfully applied in regenerative medicine in the future.

Proposals for Future Work

To extend the findings obtained in this study towards application in tissue engineering, the following topics should also be researched:

1. Effect of sheet fluidity on endothelial network formation

   In Chapter 1, the cell migration of the packed cells was revealed as sheet fluidity. It would be interesting to investigate the effect of sheet fluidity on the endothelial network formation, by changing the density, or the population balance of the packed cells.

2. Effect of cytokines on endothelial network formation

   Endothelial network formation, as the initial step of angiogenesis, is likely influenced by angiogenic factors, such as VEGF, HGF, bFGF and SDF-1. It is recommended to investigate the effect of cytokines secreted from the packed cells, or the effect of additional cytokines into the culture medium on endothelial network formation.

3. Maturation of endothelial network formation using pericytes

   In the present research, the primitive endothelial network gradually degraded after four or five days. Therefore, it would be interesting to advance this research by considering the question of how to fabricate more complicated stable endothelial tubes as capillaries with biological functions by adding pericytes.

4. Application of the model in angiogenesis research and tissue engineering

   The 3D *in vitro* model with quantitative analysis using image processing in this study could be applied in angiogenesis research, e.g., testing antiangiogenic factors. The endothelial network formed in 3D engineered tissue as prevascularization is also a promising tissue which might improve the survival rate of the cell sheet transplanted to the host. It would be interesting to investigate the integration of this endothelial network with the blood vessels of the host.

Nomenclature

$\bar{D}_{\mathrm{O}}$	Diffusivity of overall green basal layer	[μm^2/h]
$\bar{D}_{\mathrm{M}}$	Diffusivity of green target HSMMs from basal layer	[μm^2/h]
$\bar{D}_{\mathrm{F}}$	Diffusivity of green target HDFs from basal layer	[μm^2/h]
f_{G}	Frequency of green target cells in each layer of the cell sheet	[-]
h	Thickness of the cell sheet	[μm]
L	Total length of endothelial network formation	[cm^{-1}]
L/ X_0	Specific length	[cm/cell]
L/N_{T}	Extent of endothelial network formation	[cm/tip]
N_{T}	Total tip number of endothelial network formation	[tip/cm^2]
N_{T} / X_0	Specific tip number	[tip/cell]
t	Incubation time	[h]
X_0	Initial density of HUVECs	[cells/cm^2]
X_{S}	Seeding density of HUVECs	[cells/cm^2]

Abbreviations

2D	Two-dimensional
3D	Three-dimensional
bFGF	Basic fibroblast growth factor
BSA	Bovine serum albumin
CLSM	Confocal laser scanning microscopy
DMEM	Dulbecco's modified Eagle's medium
ECs	Endothelial cells
ECM	Extracellular matrix
EGM-2	Endothelial growth media
FBS	Fetal bovine serum
GFP-HUVECs	Green fluorescent protein expressing human umbilical vein endothelial cells
HDFs	Human dermal fibroblasts
HGF	Hepatocyte growth factor
HSMMs	Human skeletal muscle myoblasts
HUVECs	Human umbilical vein endothelial cells
MI	Myocardial infarction
PBS	Phosphate buffered saline
PIPAAm	Poly-(*N*-isopropylacrylamide)
SD	Standard deviation
SDF-1	Stromal-derived factor 1
VEGF	Vascular endothelial growth factor

Literature Cited

Al Attar, N., Razak, A. B. and Scorsin, M.: Cellular transplantation: new horizons in the surgical management of heart failure. *J. R. Coll. Surg. Edinb.*, **47**, 749-752 (2002).

Almagro, S., Durmort, C., Chervin-Petinot, A., Heyraud, S., Dubois, M., Lambert, O., Maillefaud, C., Hewat, E., Schaal, J. P., Huber, P. and Gulino-Debrac, D.: The motor protein myosin-X transports VE-cadherin along filopodia to allow the formation of early endothelial cell-cell contacts. *Mol. Cell. Biol.*, **30**, 1703-1717 (2010).

Asakawa, N., Shimizu, T., Tsuda, Y., Sekiya, S., Sasagawa, T., Yamato, M., Fukai, F. and Okano, T.: Pre-vascularization of *in vitro* three-dimensional tissues created by cell sheet engineering. *Biomaterials*, **31**, 3903-3909 (2010).

Auerbach, R., Lewis, R., Shinners, B., Kubai, L. and Akhtar, N.: Angiogenesis assays: A critical overview. *Clin. Chem.*, **49**, 32-40 (2003).

Black, A. F., Berthod, F., L'Heureux, N., Germain, L. and Auger, F. A.: *In vitro* reconstruction of a human capillary-like network in a tissue-engineered skin equivalent. *FASEB J.*, **12**, 1331-1340 (1998).

Bondesen, B. A., Jones, K. A., Glasgow, W. C. and Pavlath, G. K.: Inhibition of myoblast migration by prostacyclin is associated with enhanced cell fusion. *FASEB J.*, **21**, 3338-3345 (2007).

Brown, R. A., Wiseman, M., Chuo, C. B., Cheema, U. and Nazhat, S. N.: Ultrarapid engineering of biomimetic materials and tissues: Fabrication of nano- and microstructures by plastic compression. *Adv. Funct. Mater.*, **15**, 1762-1770 (2005).

Cao, Y.: Angiogenesis: What can it offer for future medicine? *Exp. Cell Res.*, **316**, 1304-1308 (2010).

Carmeliet, P.: Angiogenesis in life, disease and medicine. *Nature*, **438**, 932-936 (2005).

Chowdhury, S. R., Muneyuki, Y., Takezawa, Y., Kino-oka, M., Saito, A., Sawa, Y. and Taya, M.: Synergic stimulation of laminin and epidermal growth factor facilitates the myoblast growth through promoting migration. *J. Biosci. Bioeng.*, **108**, 174-177 (2009).

Chowdhury, S. R., Muneyuki, Y., Takezawa, Y., Kino-oka, M., Saito, A., Sawa, Y. and Taya, M.: Growth and differentiation potentials in confluent state of culture of human skeletal muscle myoblasts. *J. Biosci. Bioeng.*, **109**, 310-313 (2010).

Coppen, S. R., Fukushima, S., Shintani, Y., Takahashi, K., Varela-Carver, A., Salem, H., Yashiro, K., Yacoub, M. H. and Suzuki, K.: A factor underlying late-phase arrhythmogenicity after cell therapy to the heart - Global downregulation of connexin43 in the host myocardium after skeletal myoblast transplantation. *Circulation*, **118**, S138-S144 (2008).

Dang, S. M., Kyba, M., Perlingeiro, R., Daley, G. Q. and Zandstra, P. W.: Efficiency of embryoid body formation and hematopoietic development from embryonic stem cells in different culture systems. *Biotechnol. Bioeng.*, **78**, 442-453 (2002).

Deasy, B. M., Lu, A., Tebbets, J. C., Feduska, J. M., Schugar, R. C., Pollett, J. B., Sun, B., Urish, K. L., Gharaibeh, B. M., Cao, B., Rubin, R. T. and Huard, J.: A role for cell sex in stem cell-mediated skeletal muscle regeneration: female cells have higher muscle regeneration efficiency. *J. Cell Biol.*, **177**, 73-86 (2007).

Duguay, D., Foty, R. A. and Steinberg, M. S.: Cadherin-mediated cell adhesion and tissue segregation: qualitative and quantitative determinants. *Dev. Biol.*, **253**, 309-323 (2003).

Esser, S., Lampugnani, M. G., Corada, M., Dejana, E. and Risau, W.: Vascular endothelial growth factor induces VE-cadherin tyrosine phosphorylation in endothelial cells. *J. Cell Sci.*, **111**, 1853-1865 (1998).

Folkman, J.: Angiogenesis in cancer, vascular, rheumatoid and other disease. *Nat. Med.*, **1**, 27-31 (1995).

Folkman, J.: Opinion - Angiogenesis: an organizing principle for drug discovery? *Nat. Rev. Drug Discov.*, **6**, 273-286 (2007).

Haider, H. K., Tan, A. C. K., Aziz, S., Chachques, J. C. and Sim, E. K. W.: Myoblast transplantation for cardiac repair: a clinical perspective. *Mol. Ther.*, **9**, 14-23 (2004).

Haraguchi, Y., Shimizu, T., Sasagawa, T., Sekine, H., Sakaguchi, K., Kikuchi, T., Sekine, W., Sekiya, S., Yamato, M., Umezu, M. and Okano, T.: Fabrication of functional three-dimensional tissues by stacking cell sheets *in vitro*. *Nat. Protoc.*, **7**, 850-858 (2012a).

Haraguchi, Y., Shimizu, T., Yamato, M. and Okano, T.: Scaffold-free tissue engineering using cell sheet technology. *RSC Adv.*, **2**, 2184-2190 (2012b).

Hassink, R. J., de la Riviere, A. B., Mummery, C. L. and Doevendans, P. A.: Transplantation of cells for cardiac repair. *J. Am. Coll. Cardiol*., **41**, 711-717 (2003).

Hata, H., Matsumiya, G., Miyagawa, S., Kondoh, H., Kawaguchi, N., Matsuura, N., Shimizu, T., Okano, T., Matsuda, H. and Sawa, Y.: Grafted skeletal myoblast sheets attenuate myocardial remodeling in pacing-induced canine heart failure model. *J. Thorac. Cardiovasc. Surg.*, **132**, 918-924 (2006).

Hawke, T. J. and Garry, D. J.: Myogenic satellite cells: physiology to molecular biology. *J. Appl. Physiol.*, **91**, 534-551 (2001).

Horwitz, R. and Webb, D.: Cell migration. *Curr. Biol.*, **13**, R756-759 (2003).

Ito, A., Shinkai, M., Honda, H. and Kobayashi, T.: Medical application of functionalized magnetic nanoparticles. *J. Biosci. Bioeng.*, **100**, 1-11 (2005).

Jawad, H., Ali, N. N., Lyon, A. R., Chen, Q. Z., Harding, S. E. and Boccaccini, A. R.: Myocardial tissue engineering: a review. *J. Tissue Eng. Regen. Med.*, **1**, 327-342 (2007).

Kino-oka, M., Agatahama, Y., Hata, N. and Taya, M.: Evaluation of growth potential of human epithelial cells by motion analysis of pairwise rotation under glucose-limited condition. *Biochem. Eng. J.*, **19**, 109-117 (2004).

Kino-oka, M., Kim, J., Kurisaka, K. and Kim, M.-H.: Preferential growth of skeletal myoblasts and fibroblasts in co-culture on a dendrimer-immobilized surface. *J. Biosci. Bioeng.*, **115**, 96-99 (2013).

Ko, H. C. H., Milthorpe, B. K. and McFarland, C. D.: Engineering thick tissues - The vascularisation problem. *Eur. Cells Mater.*, **14**, 1-18 (2007).

Kunz-Schughart, L. A., Schroeder, J. A., Wondrak, M., van Rey, F., Lehle, K., Hofstaedter, F. and Wheatley, D. N.: Potential of fibroblasts to regulate the formation of three-dimensional vessel-like structures from endothelial cells *in vitro*. *Am. J. Physiol. Cell Physiol.*, **290**, C1385-1398 (2006).

Lamalice, L., Le Boeuf, F. and Huot, J.: Endothelial cell migration during angiogenesis. *Circ. Res.*, **100**, 782-794 (2007).

Levenberg, S., Rouwkema, J., Macdonald, M., Garfein, E. S., Kohane, D. S., Darland, D. C., Marini, R., van Blitterswijk, C. A., Mulligan, R. C., D'Amore, P. A. and Langer, R.: Engineering vascularized skeletal muscle tissue. *Nat. Biotechnol.*, **23**, 879-884 (2005).

Louis, M., Zanou, N., Van Schoor, M. and Gailly, P.: TRPC1 regulates skeletal myoblast migration and differentiation. *J. Cell Sci.*, **121**, 3951-3959 (2008).

Manoussaki, D., Lubkin, S. R., Vernon, R. B. and Murray, J. D.: A mechanical model for the formation of vascular networks *in vitro*. *Acta Biotheor.*, **44**, 271-282 (1996).

Martins, G. G. and Kolega, J.: Endothelial cell protrusion and migration in three-dimensional collagen matrices. *Cell Motil. Cytoskel.*, **63**, 101-115 (2006).

Matsusaki, M., Kadowaki, K., Nakahara, Y. and Akashi, M.: Fabrication of celtular multilayers with nanometer-sized extracellular matrix films. *Angew. Chem. Int. Edit.*, **46**, 4689-4692 (2007).

Memon, I. A., Sawa, Y., Fukushima, N., Matsumiya, G., Miyagawa, S., Taketani, S., Sakakida, S. K., Kondoh, H., Aleshin, A. N., Shimizu, T., Okano, T. and Masuda, H.: Repair of impaired myocardium by means of implantation of engineered autologous myoblast sheets. *J. Thorac. Cardiov. Sur.*, **130**, 1333-1341 (2005).

Menasch, P., Alfieri, O., Janssens, S., McKenna, W., Reichenspurner, H., Trinquart, L., Vilquin, J. T., Marolleau, J. P., Seymour, B., Larghero, J., Lake, S., Chatellier, G., Solomon, S., Desnos, M. and Hagege, A. A.: The myoblast autologous grafting in ischemic cardiomyopathy (MAGIC) trial: first randomized placebo-controlled study of myoblast transplantation. *Circulation*, **117** (9), 1189-1200 (2008).

Menasche, P.: Skeletal myoblasts and cardiac repair. *J. Mol. Cell. Cardiol.*, **45**, 545-553 (2008).

Miyagawa, S., Roth, M., Saito, A., Sawa, Y. and Kostin, S.: Tissue-engineered cardiac constructs for cardiac repair. *Ann. Thorac. Surg.*, **91**, 320-329 (2011).

Mori, H., Ninomiya, K., Kanemura, Y., Yamasaki, M., Kino-oka, M. and Taya, M.: Image cytometry for analyzing regional distribution of cells inside human neurospheres. *J. Biosci. Bioeng.*, **103**, 384-387 (2007).

Munoz-Chapuli, R., Quesada, A. R. and Medina, M. A.: Angiogenesis and signal transduction in endothelial cells. *Cell. Mol. Life Sci.*, **61**, 2224-2243 (2004).

Nagai, N., Yunoki, S., Satoh, Y., Tajima, K. and Munekata, M.: A method of cell-sheet preparation using collagenase digestion of salmon atelocollagen fibrillar gel. *J. Biosci. Bioeng.*, **98**, 493-496 (2004).

Nakamura, M., Iwanaga, S., Henmi, C., Arai, K. and Nishiyama, Y.: Biomatrices and biomaterials for future developments of bioprinting and biofabrication. *Biofabrication*, **2** (1), 014110 (2010).

Okano, T., Yamada, N., Sakai, H. and Sakurai, Y.: A novel recovery system for cultured cells using plasma-treated polystyrene dishes grafted with poly(N-isopropylacrylamide). *J. Biomed. Mater. Res.*, **27**, 1243-1251 (1993).

Otsu, N.: Threshold selection method from gray-level histograms. *IEEE Trans. Syst. Man Cybern.*, **9**, 62-66 (1979).

Perez-Ilzarbe, M., Agbulut, O., Pelacho, B., Ciorba, C., Jose-Eneriz, E. S., Desnos, M., Hagege, A. A., Aranda, P., Andreu, E. J., Menasche, P. and Prosper, P.: Characterization of the paracrine effects of human skeletal myoblasts transplanted in infarcted myocardium. *Eur. J. Heart Fail.*, **10**, 1065-1072 (2008).

Pittet, P., Lee, K. M., Kulik, A. J., Meister, J. J. and Hinz, B.: Fibrogenic fibroblasts increase intercellular adhesion strength by reinforcing individual OB-cadherin bonds. *J. Cell Sci.*, **121**, 877-886 (2008).

Qiu, F., Chen, Y., Cheng, J., Wang, C., Xu, H. and Zhao, X.: A simple method for cell sheet fabrication using mica surfaces grafted with peptide detergent A(6)K. *Macromol. Biosci.*, **10**, 881-886 (2010).

Rouwkema, J., de Boer, J. and Van Blitterswijk, C. A.: Endothelial cells assemble into a 3-dimensional prevascular network in a bone tissue engineering construct. *Tissue Eng.*, **12**, 2685-2693 (2006).

Sasagawa, T., Shimizu, T., Sekiya, S., Haraguchi, Y., Yamato, M., Sawa, Y. and Okano, T.: Design of prevascularized three-dimensional cell-dense tissues using a cell sheet stacking manipulation technology. *Biomaterials*, **31**, 1646-1654 (2010).

Sawa, Y., Miyagawa, S., Sakaguchi, T., Fujita, T., Matsuyama, A., Saito, A., Shimizu, T. and Okano, T.: Tissue engineered myoblast sheets improved cardiac function sufficiently to discontinue LVAS in a patient with DCM: report of a case. *Surg. Today*, **42**, 181-184 (2012).

Sekine, H., Shimizu, T., Dobashi, I., Matsuura, K., Hagiwara, N., Takahashi, M., Kobayashi, E., Yamato, M. and Okano, T.: Cardiac cell sheet transplantation improves damaged heart function via superior cell survival in comparison with dissociated cell injection. *Tissue Eng. Part A*, **17**, 2973-2980 (2011).

Sekiya, N., Matsumiya, G., Miyagawa, S., Saito, A., Shimizu, T., Okano, T., Kawaguchi, N., Matsuura, N. and Sawa, Y.: Layered implantation of myoblast sheets attenuates adverse cardiac remodeling of the infarcted heart. *J. Thorac. Cardiov. Sur.*, **138**, 985-993 (2009).

Sekiya, N., Tobita, K., Beckman, S., Okada, M., Gharaibeh, B., Sawa, Y., Kormos, R. L. and Huard, J.: Muscle-derived stem cell sheets support pump function and prevent cardiac arrhythmias in a model of chronic myocardial infarction. *Mol. Ther.*, **21**, 662-669 (2013).

Sekiya, S., Shimizu, T., Yamato, M., Kikuchi, A. and Okano, T.: Bioengineered cardiac cell sheet grafts have intrinsic angiogenic potential. *Biochem. Bioph. Res. Co.*, **341**, 573-582 (2006).

Sekiya, S., Muraoka, M., Sasagawa, T., Shimizu, T., Yamato, M. and Okano, T.: Three-dimensional cell-dense constructs containing endothelial cell-networks are an effective tool for *in vivo* and *in vitro* vascular biology research. *Microvasc. Res.*, **80**, 549-551 (2010).

Serini, G., Ambrosi, D., Giraudo, E., Gamba, A., Preziosi, L. and Bussolino, F.: Modeling the early stages of vascular network assembly. *EMBO J.*, **22**, 1771-1779 (2003).

Simons, M.: Angiogenesis - Where do we stand now? *Circulation*, **111**, 1556-1566 (2005).

Singec, I., Knoth, R., Meyer, R. P., Maciaczyk, J., Volk, B., Nikkhah, G., Frotscher, M. and Snyder, E. Y.: Defining the actual sensitivity and specificity of the neurosphere assay in stem cell biology. *Nat. Methods.*, **3**, 801-806 (2006).

Takezawa, T., Takeuchi, T., Nitani, A., Takayama, Y., Kino-oka, M., Taya, M. and Enosawa, S.: Collagen vitrigel membrane useful for paracrine assays *in vitro* and drug delivery systems *in vivo*. *J. Biotechnol.*, **131**, 76-83 (2007).

Taylor, D. A., Atkins, B. Z., Hungspreugs, P., Jones, T. R., Reedy, M. C., Hutcheson, K. A., Glower, D. D. and Kraus, W. E.: Regenerating functional myocardium: improved performance after skeletal myoblast transplantation. *Nat. Med.*, **4**, 929-933 (1998).

Timmins, N. E., Dietmair, S. and Nielsen, L. K.: Hanging-drop multicellular spheroids as a model of tumour angiogenesis. *Angiogenesis*, **7**, 97-103 (2004).

Tsigkou, O., Pomerantseva, I., Spencer, J. A., Redondo, P. A., Hart, A. R., O'Doherty, E., Lin, Y. F., Friedrich, C. C., Daheron, L., Lin, C. P., Sundback, C. A., Vacanti, J. P. *et al.*: Engineered vascularized bone grafts. *P. Natl. Acad. Sci. USA*, **107**, 3311-3316 (2010).

Underwood, P. A., Bean, P. A. and Gamble, J. R.: Rate of endothelial expansion is controlled by cell: cell adhesion. *Int. J. Biochem. Cell Biol.*, **34**, 55-69 (2002).

Unger, R. E., Sartoris, A., Peters, K., Motta, A., Migliaresi, C., Kunkel, M., Bulnheim, U., Rychly, J. and Kirkpatrick, C. J.: Tissue-like self-assembly in cocultures of endothelial cells and osteoblasts and the formation of microcapillary-like structures on three-dimensional porous biomaterials. *Biomaterials*, **28**, 3965-3976 (2007).

van der Meer, A. D., Vermeul, K., Poot, A. A., Feijen, J. and Vermes, I.: A microfluidic wound-healing assay for quantifying endothelial cell migration. *Am. J. Physiol. Heart Circ. Physiol.*, **298**, H719-H725 (2010).

Vernon, R. B. and Sage, E. H.: A novel, quantitative model for study of endothelial cell migration and sprout formation within three-dimensional collagen matrices. *Microvasc. Res.*, **57**, 118-133 (1999)..

Wang, W., Pan, H. Y., Murray, K., Jefferson, B. S. and Li, Y.: Matrix metalloproteinase-1 promotes muscle cell migration and differentiation. *Am. J. Pathol.*, **174**, 541-549 (2009).

Wood, W. and Martin, P.: Structures in focus - filopodia. *Int. J. Biochem. Cell Biol.*, **34**, 726-730 (2002).

Yang, J., Yamato, M., Kohno, C., Nishimoto, A., Sekine, H., Fukai, F. and Okano, T.: Cell sheet engineering: recreating tissues without biodegradable scaffolds. *Biomaterials*, **26**, 6415-6422 (2005).

Yang, J., Yamato, M., Shimizu, T., Sekine, H., Ohashi, K., Kanzaki, M., Ohki, T., Nishida, K. and Okano, T.: Reconstruction of functional tissues with cell sheet engineering. *Biomaterials*, **28**, 5033-5043 (2007).

List of Publications

Original Papers:

1. Ngo, T. X., Nagamori, E., Kikuchi, T., Shimizu, T., Okano, T., Taya, M., and Kino-oka, M.: Endothelial cell behavior inside myoblast sheets with different thickness, *Biotechnol. Lett.*, **35** (7), 1001-1008 (2013).
2. Nagamori, E., Ngo, T. X., Takezawa, Y., Saito, A., Sawa, Y., Shimizu, T., Okano, T., Taya, M., and Kino-oka, M.: Network formation through active migration of human vascular endothelial cells in a multilayered skeletal myoblast sheet, *Biomaterials*, **34** (3), 662-668 (2013).
3. Kino-oka, M., Ngo, T. X., Nagamori, E., Takezawa, Y., Miyake, Y., Sawa, Y., Saito, A., Shimizu, T., Okano, T., and Taya, M.: Evaluation of vertical cell fluidity in a multilayered sheet of skeletal myoblasts, *J. Biosci. Bioeng.*, **113** (1), 128-131 (2012).

International conference proceedings:

1. Ngo, T. X., Nagamori, E., Taya, M., and Kino-oka, M.: Network formation through active migration of human vascular endothelial cells in a multilayered skeletal myoblast sheet, The 25th Annual and International Meeting of Japanese Association for Animal Cell Technology (JAACT), P-74 (2012).
2. Kino-oka, M., Ngo, T. X., and Taya, M.: Novel method for quality control of myoblast sheet toward clinical transplantation, American Institute of Chemical Engineers (AIChE) Annual Meeting, 625Y (2011).

Acknowledgements

First of all, I would like to express my deepest gratitude to my supervisor, Prof. Masahito Taya (Division of Chemical Engineering, Graduate School of Engineering Science, Osaka University) for giving me the precious opportunity to study at Osaka University, for all of his continuous support, crucial guidance and valuable advice for my study and life in Japan.

I would like to express my sincerest appreciation to my co-supervisor, Prof. Masahiro Kino-oka (Department of Biotechnology, Graduate School of Engineering, Osaka University) for kindly providing me, with the best conditions to carry out this research in his laboratory. I have been deeply touched by his philosophy of life and research. With his strict, meticulous, and expert instruction, I have gained and progressed greatly throughout my Doctoral course.

I also would like to express my honest thankfulness to Associate Prof. Eiji Nagamori (Kino-oka Laboratory), my research advisor, for his patience, understanding, constructive criticism and support in both life and research.

I would like to express my sincere appreciation to Prof. Hiroshi Umakoshi (Division of Chemical Engineering, Graduate School of Engineering Science, Osaka University) for his crucial comments and questions that helped me to polish this thesis.

I would also like to express my sincere gratefulness to Associate Prof. Shinji Sakai, Assistant Prof. Yoshihiro Ojima (Taya Laboratory), Assistant Prof. Mee-Hae Kim (Kino-oka Laboratory), Dr. Yoshinori Takezawa, Dr. Masrina binti Mohd Nadzir, and Dr. Kei Kanie for their academic advice on my research. I also owe special thanks to all the members of the Cell Sheet Group, especially Ms. Rieko Ami, Ms. Yasuki Miyake, Mr. Masashi Oda and Ms. Yingzi Zhao for their initial training and cooperation; to the members of the Simulation Group,

especially Mr. Shingo Uratochi, Mr. Shota Ohno, Mr. Sojiro Ohta and Ms. Kyoko Kishi, for their excellent analysis software; and to all the other members of the Taya and Kino-oka Laboratory, especially Ms. Nguyen Hong Minh, Mr. Tomoaki Ashida, Mr. Naoki Tsubakino, Ms. Nao Maruyama, Mr. Kohji Yamada, Mr. Yuuki Ogawa and Ms. Rie Sonoi for their kind help in making my lab life exciting and unforgettable.

I also express my gratefulness to Ms. Masako Karita, Ms. Hiroko Goto, Ms. Mitsuko Wakamatsu, Ms Kaori Ishida (secretaries of Taya and Kino-oka Laboratory), Ms. Emiko Tasaka (International Student Center, Graduate School of Engineering Science), Ms. Akiko Otsuki (Japanese teacher), my host family, and all of my international and Vietnamese friends for their hearty support.

I would like to express my appreciation to the Japanese Ministry of Education, Culture, Sports, Science and Technology for giving me the opportunity to do my PhD as a MEXT scholar at Osaka University.

Very special thanks go my family, especially my wife Tran Thi Bich Phuong and my uncle Ngo Xuan Kien, for their love, understanding and inspiration, and to Nguyen Hoang Minh, my best friend, who has always spiritually encouraged me to pursue the academic dream!

Ngo Xuan Trung

Division of Chemical Engineering

Graduate School of Engineering Science

Osaka University, Osaka, JAPAN

September, 2013